A Mechano-Electrochemical Model of Radial Deformation of the Capillary Glycocalyx

Edward R. Damiano* and Thomas M. Stace*†

*Department of Mechanical and Industrial Engineering, University of Illinois at Urbana-Champaign, Urbana, Illinois 61801 USA and †Cavendish Laboratory, University of Cambridge, Cambridge CB3 0HE, United Kingdom

ABSTRACT A mechano-electrochemical theory of the surface glycocalyx on capillary endothelial cells is presented that models the structure as a mixture of electrostatically charged macromolecules hydrated in an electrolytic fluid. Disturbances arising from mechanical deformation are introduced as perturbations away from a nearly electroneutral equilibrium environment. Under mechanical compression of the layer, such as might occur on the passing of stiff leukocytes through capillaries, the model predicts that gradients in the electrochemical potential of the compressed layer cause a redistribution of mobile ions within the glycocalyx and a rehydration and restoration of the layer to its equilibrium dimensions. Because of the large deformations of the glycocalyx arising from passing leukocytes, nonlinear kinematics associated with finite deformations of the layer are accounted for in the theory. A pseudo-equilibrium approximation is invoked for the transport of the mobile ions that reduces the system of coupled nonlinear integro-differential equations to a single nonlinear partial differential equation that is solved numerically for the compression and recovery of the glycocalyx using a finite difference method on a fixed grid. A linearized model for small strains is also obtained as verification of the finite difference solution. Results of the asymptotic analysis agree well with the nonlinear solution in the limit of small deformations of the layer. Using existing experimental and theoretical estimates of glycocalyx properties, the glycocalyx fixed-charge density is estimated from the analysis to be ~1 mEq/l, i.e., we estimate that there exists approximately one fixed charge on the glycocalyx for every 100 ions in blood. Such a charge density would result in a voltage differential between the undeformed glycocalyx and the capillary lumen of ~0.1 mV. In addition to providing insight into the mechano-electrochemical dynamics of the layer under deformation, the model suggests several methods for obtaining improved estimates of the glycocalyx fixed-charge density and permeability in vivo.

INTRODUCTION

In a recent study, we investigated the influence of the anionic fixed-charge groups bound to the capillary glycocalyx on the electrochemical transport of charged molecules through the glycocalyx (Stace and Damiano, 2001). However, no attempt has been made to analyze the role of these fixed-charge groups on deformations of the glycocalyx matrix such as would arise in the presence of a passing leukocyte through the capillary. In this paper, we build upon the previous electrochemical model and extend the analysis to address transient mechanical deformations of the glycocalyx surface layer. Recent speculation as to the origins of the restoring forces in the capillary glycocalyx has raised attention to a variety of possible sources including elastic-restoring mechanisms, osmotic and oncotic pressures, electrostatic potentials, and fluid dynamical mechanisms (Damiano et al., 1996; Damiano, 1998; Secomb et al., 1998, 2001; Feng and Weinbaum, 2000). New experimental approaches to observing the glycocalyx in vivo have revealed what appears to be the time course of the layer's dynamic response to transient deformations by passing leukocytes (Vink et al., 1999). In the analysis presented here, we develop a mechano-electrochemical model of the glycocalyx, which presumes that, under deformation, electrostatic potentials arising from the fixed charges bound to the solid matrix and concentration gradients arising from a redistribution of the glycocalyx molecules are the predominant mechanisms responsible for the layer's tendency to restore itself to its equilibrium configuration.

The possible relevance of the glycocalyx to microcirculatory function was first considered by Copley and Silberberg (Lahav et al., 1973; Krindel and Silberberg 1979; Copley 1974). Klitzman and Duling (1979) implicated the glycocalyx in accounting for the low capillary tube hematocrits (i.e., the instantaneous volume fraction of red cells resident in the capillary) they observed in capillaries of skeletal muscle. Evidence that the macromolecules of the glycocalyx might interfere with flow in a large plasma layer near the capillary wall was first reported by Desjardins and Duling (1990). After enzyme treatment targeted at cleaving specific proteoglycan molecules within the glycocalyx, they observed a two-fold increase in capillary tube hematocrit. Using a light–dye treatment to remove the glycocalyx, Vink and Duling (1996) observed a similar trend in tube hematocrit and obtained the first estimate of the thickness of the layer in vivo.

Combining network simulations with measurements of blood flow in large-scale microvascular networks, Pries et al. (1994) concluded that the resistance to blood flow in microvessels between 10 and 30 μm in diameter was dramatically higher than in glass tubes of the same diameter. In

Submitted March 26, 2001, and accepted for publication November 16, 2001.

Address reprint requests to E. R. Damiano, Dept. of Mechanical and Industrial Engineering, Univ. of Illinois at Urbana-Champaign, 140 Mechanical Engineering Bldg., 1206 West Green St., Urbana, IL 61801. Tel.: 217-333-6107; Fax: 217-244-6534; E-mail: damiano@uiuc.edu.

© 2002 by the Biophysical Society

0006-3495/02/03/1153/23 $2.00

a more recent study, Pries et al. (1997) found that the resistance to blood flow in microvascular networks decreased markedly after enzyme treatment to remove the glycocalyx. These studies, and those of Duling and coworkers, suggest that the glycocalyx could serve to retard plasma flow near the vessel wall, which, in turn, would result in enhanced resistance to blood flow and lower capillary tube hematocrits in vivo than in smooth glass tubes.

Until recently, all theoretical models of red-cell motion through capillaries in the single-file flow regime completely neglected the endothelial-cell glycocalyx. Most of these models approximated the capillary as a rigid, smooth-walled, uniform circular cylinder. Results of these studies, which were derived from either finite element analyses (Zarda et al., 1977a,b; Özkaya, 1986) or models that invoked the lubrication-theory approximation (Secomb and Gross 1983; Özkaya, 1986; Secomb et al., 1986), were found to be in good agreement with experimental observations of blood flow through narrow glass tubes (Özkaya, 1986; Secomb et al., 1986; Skalak and Özkaya, 1987; Secomb, 1995). None of these models, however, compared favorably with in vivo observations of blood flow in microvascular networks (Pries et al., 1994).

Among the earliest analytical attempts to investigate flow through the glycocalyx came with the work of Barry et al. (1991). Their work considered steady and unsteady flow of a Newtonian fluid in a channel lined with a poroelastic wall layer. Wang and Parker (1995) applied mixture theory and two-dimensional lubrication theory to the problem of a sphere falling through a quiescent fluid in a cylindrical tube lined with a deformable porous wall layer. Damiano et al. (1996) provided the first analytical solutions of axisymmetric pressure-driven flow of rigid close-fitting particles in a cylindrical tube lined with a poroelastic wall layer. Damiano (1998) incorporated the axisymmetric model developed by Damiano et al. (1996) into the first realistic model of capillary blood flow that accounts for the effects of the endothelial-cell glycocalyx and the deformation of the red-cell membrane. Secomb et al. (1998, 2001) went further to include the effects of membrane viscosity and membrane bending and shear elasticities in the red cell. Although these models represent a significant improvement over existing theories of capillary rheology, the characterizations of the glycocalyx developed by Damiano (1998) and Secomb et al. (1998, 2001) are rather simplistic and only capture the gross rheological effects of plasma retardation near the capillary wall. In particular, effects of the electrostatic properties of the layer on glycocalyx permeability and deformation have not been addressed in a rigorous analytical model. One of the most compelling reasons to pursue this stems from recent in vivo investigations into the mechanical properties (Vink et al., 1999) and molecular transport characteristics (Henry and Duling, 1999, 2000; Vink and Duling, 2000) of the glycocalyx.

Preliminary experiments of Vink et al. (1999) reveal important information about the mechanical response of the glycocalyx to deformation. Because leukocytes are larger and much stiffer than red blood cells, they occupy more of the capillary lumen. In both in vitro and in vivo studies, extremely thin lubrication layers are observed between the leukocyte membrane and the vessel wall (Needham and Hochmuth, 1990; Vink and Duling, 1996). As a consequence of this, leukocytes travel more slowly through capillaries than do red cells, which likely accounts, in part, for the commonly observed train of red blood cells that often follows a tightly fitting leukocyte (Vink et al., 1999). In capillaries less than 7 μm in diameter, it appears as if the glycocalyx experiences large deformations on the passing of individual leukocytes (Vink et al., 1999). The red cells immediately behind the leukocyte are maximally expanded and fill most of the capillary lumen. As red blood cells from upstream move into the field of view, they become progressively more deformed, presumably as a result of the restoring forces of the glycocalyx as it swells back to its equilibrium configuration. In preliminary studies of Vink et al. (1999), the recovery time of the compressed glycocalyx matrix has been measured in the wake of a passing leukocyte and was reported as being $\sim$1 s. The recovery time was based on the time required for the mean diameter of red cells upstream of the leukocyte to reach a steady-state value.

On the basis of these observations, we seek to develop a mechano-electrochemical model of the glycocalyx that assumes that the layer consists of a multicomponent mixture of an incompressible fluid, an anionic porous deformable matrix, and mobile cations and anions. At time $t = t_0$, the concentration distribution in the reference configuration is denoted by $c^{\mathrm{F}}(\mathbf{X}, t_0) = c^{\mathrm{F}}(\mathbf{x}, t_0)$, where the components of $\mathbf{x}$ are the spatial coordinates, and the components of $\mathbf{X}$ are the reference coordinates of a material point in the field. The fixed-charge density, $nc^{\mathrm{F}}(\mathbf{X}, t)$, where $-n$ is the mean molecular valence of the glycocalyx, is assumed to be directly proportional to the solid-matrix concentration distribution at any time, t. Although the fixed-charge groups per unit mass of the solid matrix are assumed to be constant, their concentration distribution can change with deformation of the solid matrix. Thus, nc^{F} depends upon the initial concentration distribution in the reference configuration and the state of deformation of the solid matrix. In equilibrium, the mobile ions establish concentration distributions, $c^{+}(\mathbf{X}, t_0)$ and $c^{-}(\mathbf{X}, t_0)$, that nearly counterbalance the fixed charges on the solid matrix. In equilibrium, complete electroneutrality is not achieved everywhere because that would result in large gradients in the ion distributions. Instead, the ion concentrations assume distributions in equilibrium that result in a nonzero electric field and nonzero chemical potential gradients, but which minimize the equilibrium electrochemical potential gradient of the system as a whole. When integrated over the vessel cross section, however, these local charge imbalances cancel such that global

space–charge neutrality exists within the capillary. Because of these local charge imbalances and concentration gradients that exist in equilibrium, a state of tension sets up in the matrix that balances the electrochemical forces in the glycocalyx. Thus, the energy required to maintain the static electric field and nonuniform distributions in the ion concentrations is stored as tension in the matrix in equilibrium. Under compression of the layer by a passing leukocyte, an external stress traction is exerted by the cell at the apical end of the glycocalyx and the tension in the matrix is largely relieved. As the layer deforms, an imbalance exists between the externally applied stress traction and the electrochemical forces in the matrix. Upon recovery of the compressed matrix, the electrochemical forces that restore the layer to its equilibrium configuration are resisted by permeation-induced hydraulic drag of the layer as it moves through the plasma.

A principal result of the analysis that follows is the reduced momentum equation for the displacement of the glycocalyx solid matrix. It is shown that, under purely radial deformations of the glycocalyx, the kinematically related circumferential and radial principal stretch ratios, λ_θ and $\lambda_r = \partial(R\lambda_\theta)/\partial R$, associated with a material point in the glycocalyx solid matrix are governed by

$$\frac{\lambda_r}{k}\frac{\partial(R\lambda_\theta)}{\partial t} = \frac{\partial}{\partial R}\left(T_0(R)\frac{\lambda_r}{\lambda_\theta}\right) + \frac{T_0(R)}{R}\left(\frac{\lambda_r^2}{\lambda_\theta^2} - 1\right) - c^F\frac{\partial \mu_{ec}^s}{\partial R}$$

$$a_0 \le R \le R_0, \quad (1)$$

where the electrochemical potential gradient of the glycocalyx in a monovalent salt solution is given by

$$\frac{\partial \mu_{ec}^s}{\partial R} = \frac{\partial}{\partial R}\left(\ln\left[\frac{c^F}{c_0^F}\left(\frac{c^+}{c_0^+}\right)^{n/z^+}\right]\right). \quad (2)$$

Here, R is the radial coordinate in a Lagrangian cylindrical coordinate frame, where $R = R_0$ and $R = a_0$ are, respectively, material points in the reference configuration of the solid matrix at the vessel wall and at the glycocalyx interface with the plasma in the lumen. Through the conservation of mass, the normalized glycocalyx concentration, c^F/c_0^F, is kinematically related to the principal stretch ratios (in inverse proportion to the product $\lambda_r\lambda_\theta$), and by invoking the so-called pseudo-equilibrium approximation, the normalized cation concentration, c^+/c_0^+, is algebraically related to c^F/c_0^F. Finally, in Eq. 1, $T_0(R)$ is the spatially varying isotropic tension in the glycocalyx solid matrix in the reference configuration, and k is the local permeability of the glycocalyx to water.

The mechano-electrochemical dynamics described above are embodied in the relatively simple result given by Eq. 1. The restoring force is accounted for by the last term on the right-hand side and is associated with the electrochemical potential gradient of the glycocalyx. In the reference configuration, the term on the left-hand side vanishes and the last term on the right-hand side balances the remaining terms, which are associated with the divergence in the elastic stress tensor of the matrix. During recovery of the matrix after compression, the electrochemical potential gradient dominates over the tension in the matrix and restores the layer to its equilibrium configuration. The term on the left-hand side, associated with permeation-induced drag of the solid matrix through the fluid, resists this recovery and opposes the mechano-electrochemical restoring force. As the layer rehydrates and approaches the reference configuration, the left-hand side tends toward zero until, finally, equilibrium is reestablished when the terms on the right-hand side are once again in balance.

In what follows, the conservation equations for a specialized quaternary mixture will be presented and constitutive relations will be proposed for each of its constituents. In deriving our constitutive equations, we shall assume that the glycocalyx is an extremely diffuse, anionic mucopolysaccharide that is devoid of collagen and has essentially no elastic restoring capability. The only mechanical stress we will assume the matrix itself can support is one of tension. We will therefore assume that the restoring mechanisms of the glycocalyx have their origins in electrochemical rather than elastic forces and that the fixed-charge density and chemical potential of the layer are the fundamental determinants of that restoring force. To address finite deformations of the glycocalyx, the governing equations, together with Gauss's law from electrostatics, will be formulated in Lagrangian variables for the special case of purely radial axisymmetric deformations in the absence of an axial flow through the capillary. We then invoke the assumption that the transport of mobile ions occurs as a pseudo-equilibrium process such that many of the relationships derived by Stace and Damiano (2001) for the case of a static-charge distribution can be adapted to the problem with deformation. The justification for this assumption lies in the realization that the cation concentration in blood is likely to be very large when compared with the glycocalyx fixed-charge density. As such, even large physiologic deformations of the layer result in only small perturbations to the cation concentration field which re-distributes itself quickly relative to the glycocalyx molecules by virtue of the relatively large diffusion coefficient associated with the cations. This approximation significantly simplifies the model, making it much more tractable to numerical and asymptotic analysis. Results of the analysis are presented and discussed in terms of the mechano-electrochemical dynamics of the layer under compression and recovery and the dependence of those dynamics on the parameters in the model. From our results, an estimate of the glycocalyx fixed-charge density is made based on the limited experimental data available. We conclude with a discussion of new experimental approaches inspired by the model that could be taken to obtain more precise bounds on the mechano-electrochemical properties of the structure in vivo.

THE MODEL

Using mixture theory, the glycocalyx is modeled as a multicomponent material continuum that consists of four interacting and interpenetrating constituents, which include the interstitial fluid (blood plasma), the electrostatically charged proteoglycan/glycoprotein/glycosaminoglycan solid matrix, and the mobile ions (cations and anions). Mixture theory approximates multicomponent materials as a continuum using a macroscopic field theory description (Truesdell and Toupin, 1960; Bowen, 1976; Lai et al., 1991). Also known as the theory of heterogeneous or superimposed material continua, mixture theory assumes that every spatial point in the field is occupied simultaneously by a material point of all of the constituents in the mixture. In essence, the microscale substructure is smeared or mixed throughout the material. The theory accounts not only for the intrinsic constitutive behavior of each of the components of the mixture, but it also accounts for the transfer of momentum that occurs between constituents. This momentum transfer, characterized by momentum supply forces in the conservation equations, arises from the local interaction between constituents as they move relative to each other. The model proposed here for the glycocalyx is consistent with the so-called "triphasic" theory developed by Lai et al. (1991) in the absence of an elastic-restoring capability by the matrix and in the limit as the solid-volume fraction approaches zero. The validity of invoking a continuum mixture approximation in this context is discussed in Stace and Damiano (2001).

The conservation equations

The glycocalyx will be modeled as an isotropic quaternary mixture of a solid (s), water (w), cationic ($+$), and anionic ($-$) constituent. We denote the velocity vectors of these constituents by $\mathbf{v}^{\mathrm{s}}$, $\mathbf{v}^{\mathrm{w}}$, $\mathbf{v}^{+}$, and $\mathbf{v}^{-}$, and the partial Cauchy stress tensors by $\boldsymbol{\sigma}^{\mathrm{s}}$, $\boldsymbol{\sigma}^{\mathrm{w}}$, $\boldsymbol{\sigma}^{+}$, and $\boldsymbol{\sigma}^{-}$. We shall assume that the momentum supply force exerted by one constituent on another is proportional to the relative velocity between the two constituents and that the momentum supply forces acting between two constituents are equal but opposite. The coefficient of proportionality is the frictional drag coefficient between two constituents. For the interaction between the solid and water constituents, the frictional drag coefficient corresponds to the hydraulic resistivity, which is inversely proportional to the matrix permeability to water. The frictional drag coefficient associated with the interaction between the ionic and water constituents is related to the Stokes viscous drag coefficient of an ion in solution. Because we are assuming that the volume fractions of the solid and ionic constituents are negligible, the drag forces associated with ion–ion interactions and ion–matrix interactions will be neglected. All constituents are assumed to be neutrally buoyant, and, therefore, the only body force that arises is due to the electric field, $\mathbf{E}$, induced by the fixed charges bound to the solid matrix. Finally, because the flow through the glycocalyx during physiologic deformations of the layer resides in the extremely low-Reynolds number regime, inertial terms in the momentum equations are negligible compared with surface, body, and momentum supply forces. In light of these assumptions, the momentum conservation equations for the solid, fluid, cationic, and anionic constituents are given respectively by

$$\nabla \cdot \boldsymbol{\sigma}^{\mathrm{s}} - \frac{1}{k}(\mathbf{v}^{\mathrm{s}} - \mathbf{v}^{\mathrm{w}}) - nqc^{\mathrm{F}}\mathbf{E} = \mathbf{0}, \tag{3}$$

$$\nabla \cdot \boldsymbol{\sigma}^{\mathrm{w}} + \frac{1}{k}(\mathbf{v}^{\mathrm{s}} - \mathbf{v}^{\mathrm{w}}) + f_{\mathrm{d}}^{+}\mathbf{J}^{+} + f_{\mathrm{d}}^{-}\mathbf{J}^{-} = \mathbf{0}, \tag{4}$$

and

$$\nabla \cdot \boldsymbol{\sigma}^{\pm} - f_{\mathrm{d}}^{\pm}\mathbf{J}^{\pm} + z^{\pm}qc^{\pm}\mathbf{E} = \mathbf{0}, \tag{5}$$

where the flux vectors, $\mathbf{J}^{+}$, between the mobile cations and the water constituent, and $\mathbf{J}^{-}$, between the mobile anions and the water constituent, are defined such that

$$\mathbf{J}^{\pm} = c^{\pm}(\mathbf{v}^{\pm} - \mathbf{v}^{\mathrm{w}}). \tag{6}$$

The parameter k in Eqs. 3 and 4 is the permeability of the layer to water, which is inversely proportional to the hydraulic resistivity and may depend locally on the strain field.

Summing Eqs. 3–5, we obtain the conservation of momentum for the mixture as a whole given by

$$\nabla \cdot \boldsymbol{\sigma}^{\mathrm{T}} + q\delta\mathbf{E} = \mathbf{0}, \tag{7}$$

where

$$\delta(\mathbf{x}, t) = z^{+}c^{+}(\mathbf{x}, t) + z^{-}c^{-}(\mathbf{x}, t) - nc^{\mathrm{F}}(\mathbf{x}, t) \tag{8}$$

and

$$\boldsymbol{\sigma}^{\mathrm{T}} = \boldsymbol{\sigma}^{\mathrm{s}} + \boldsymbol{\sigma}^{\mathrm{w}} + \boldsymbol{\sigma}^{+} + \boldsymbol{\sigma}^{-} = -p\mathbf{I} + \boldsymbol{\sigma}^{\mathrm{E}}. \tag{9}$$

Electrostatic effects enter as body forces rather than surface tractions as is evident from Eq. 7. In the second of Eq. 9, p accounts for the mechanical and osmotic pressures, and $\boldsymbol{\sigma}^{\mathrm{E}}$ accounts for the tensile stress stored in the solid matrix in equilibrium and during deformation of the glycocalyx. We have neglected the contribution to the total stress tensor, $\boldsymbol{\sigma}^{\mathrm{T}}$, of viscous stresses associated with $\boldsymbol{\sigma}^{\mathrm{w}}$. For length scales characteristic of flow within the glycocalyx, previous studies have suggested that viscous drag forces associated with fluid-velocity gradients are likely to be small relative to permeation-induced viscous drag forces associated with fluid motion relative to the solid matrix (Damiano et al., 1996; Damiano, 1998; Secomb et al., 1998; Feng and Weinbaum, 2000). As such, we neglect dissipative losses associated with the deviatoric or viscous stress tensor of the water constituent. This approximation is commonly made in models of articular cartilage based on mixture theory when

the prevailing flow direction is normal rather than tangential to the boundaries of the mixture (Mow et al., 1980; Lai and Mow, 1980).

Modeling the water constituent of the glycocalyx as incompressible with a volume fraction near unity, the continuity equation for the water is given by

$$\nabla \cdot \mathbf{v}^{w} = 0. \tag{10}$$

The instantaneous system boundaries of the mixture are defined by the deformed configuration of the solid matrix. As such, a flux of water across the system boundaries occurs during compression and recovery of the layer. Thus, we regard the mixture as highly compressible despite the fact that its primary constituent, taken by itself, is incompressible.

For the solid constituent, the mass density, ρ^{s}, and molecular concentration, c^{F}, are governed by the conservation of mass given by

$$\rho^{s}(\mathbf{X}, t_0) = J\rho^{s}(\mathbf{X}, t) \Rightarrow c^{F}(\mathbf{X}, t_0) = Jc^{F}(\mathbf{X}, t), \tag{11}$$

where t_0 corresponds to a time when the glycocalyx is in its reference configuration and $J = \det \mathbf{F}$ is the Jacobian of the deformation gradient tensor, $\mathbf{F} = \partial\mathbf{x}/\partial\mathbf{X}$. In addition to the continuity equations for the solid and fluid constituents, given by Eqs. 10 and 11, we impose the mass conservation equations for the mobile ions, given by

$$\frac{Dc^{\pm}}{Dt} = -\nabla \cdot \mathbf{J}^{\pm}. \tag{12}$$

Using Gauss's law from electrostatics, the electric field is governed by

$$\nabla \cdot \mathbf{E} = -\nabla^2 V = \frac{q\delta}{\epsilon}, \tag{13}$$

where δ is given by Eq. 8, the voltage, V, is the scalar electrostatic potential function, q is the elementary charge, and ϵ is the permittivity of water.

Specification of constitutive equations for $\boldsymbol{\sigma}^{s}$, $\boldsymbol{\sigma}^{w}$, $\boldsymbol{\sigma}^{+}$, $\boldsymbol{\sigma}^{-}$, $\boldsymbol{\sigma}^{E}$, and k provides a closed system of equations, which includes four scalar continuity equations, Gauss's law, and the definition of δ (Eqs. 8, 10, 11, 12, and 13) in the six scalar unknowns, c^{+}, c^{-}, c^{F}, p, V, and δ, and four vector momentum equations (Eqs. 3, 4, and 5), in the four vector unknowns, $\mathbf{v}^{s}$, $\mathbf{v}^{w}$, $\mathbf{v}^{+}$, and $\mathbf{v}^{-}$.

Physicochemical constitutive equations

In addition to the conservation equations for the mixture given above, constitutive relationships are needed to characterize the partial stress tensors of each of the constituents. For ideal solutions, or in the limit of infinite dilution, the van't Hoff equation for the osmotic pressure is analogous to the ideal gas law for the thermodynamic pressure (Katchalsky and Curran, 1965). Because the NaCl concentration in blood plasma is dilute (approximately 0.14 M, which is more than two orders of magnitude lower than the concentration of the solvent), we invoke the van't Hoff equation for the mobile ions and take

$$\frac{\pi^{\pm}}{c^{\pm}} = k_B T, \tag{14}$$

where $\pi^{\pm}$ corresponds to the osmotic pressure of the ions in solution, k_B is Boltzmann's constant, and T is absolute temperature. Under isothermal conditions, then, the ratio of the osmotic pressure to the concentration remains constant. By modeling the cationic and anionic constituents as ideal inviscid fluids, their partial Cauchy stress tensors are given by

$$\boldsymbol{\sigma}^{\pm} = -\pi^{\pm}\mathbf{I} = -k_B T c^{\pm}\mathbf{I}$$
$$\Rightarrow \nabla \cdot \boldsymbol{\sigma}^{\pm} = -k_B T \nabla c^{\pm} = -c^{\pm}\nabla\mu^{\pm}, \tag{15}$$

where, for ideal solutions, the chemical potential, $\mu^{\pm}$, of the ions is related to the ion concentration according to

$$\mu^{\pm} = \mu_0^{\pm} + k_B T \ln c^{\pm}$$
$$\Rightarrow \nabla\mu^{\pm} = k_B T \nabla \ln c^{\pm} = \frac{k_B T}{c^{\pm}} \nabla c^{\pm}. \tag{16}$$

Here, $\mu_0^{\pm}$, which depends only on temperature, is the chemical potential in the standard state (Katchalsky and Curran, 1965).

By assuming ideal behavior, Eq. 15 effectively neglects long-range Coulombic interactions between ions, which, nevertheless exist even in dilute solutions (Bockris and Reddy, 1970). To account for this departure from ideal behavior, activity coefficients, γ^{+} and γ^{-} (corresponding to the Na^{+} and Cl^{-} ions at concentrations equal to that of normal saline), are introduced as multiplicative factors in the argument of the natural logarithm appearing in Eq. 16. These activity coefficients, in general, depend on the local concentration (Robinson and Stokes, 1955). However, by Eq. 16, it is evident that only gradients in the chemical potential appear in the conservation equations governing the mobile ions. For our purposes, then, the departure from ideal behavior is dependent only upon $\nabla\gamma^{\pm} = (\partial\gamma^{\pm}/\partial c^{\pm})\nabla c^{\pm}$, and is negligible if $\partial\gamma^{\pm}/\partial c^{\pm} \ll \gamma^{\pm}/c^{\pm}$ (Bockris and Reddy, 1970). For normal saline at 310 K, this condition is met if $\partial\gamma^{\pm}/\partial c^{\pm} \ll 5$ (Robinson and Stokes, 1955). Recalling our assumption that physiological deformations of the glycocalyx induce only small perturbations in the mobile ion concentrations, it follows that the variation in $\gamma^{\pm}$ with respect to $c^{\pm}$, which, in this context, is not likely to exceed 0.01, can safely be neglected. We therefore assert that the approximation implied by Eq. 15 is reasonable despite the long-range Coulombic interactions that undoubtedly arise.

For the solid matrix, we again assume ideal gas behavior and invoke the van't Hoff equation. The chemical potential, μ^s, is thus taken to be

$$\mu^s = \mu_0^s + k_B T \ln c^F. \tag{17}$$

Introducing an extra stress, denoted by $\boldsymbol{\sigma}^E$, that accounts for the tension stored in the solid matrix, the partial Cauchy stress tensor, $\boldsymbol{\sigma}^s$, is given by

$$\boldsymbol{\sigma}^s = -k_B T c^F \mathbf{I} + \boldsymbol{\sigma}^E$$

$$\Rightarrow \nabla \cdot (\boldsymbol{\sigma}^s - \boldsymbol{\sigma}^E) = -k_B T \nabla c^F = -c^F \nabla \mu^s. \tag{18}$$

Expressing the divergence of the partial Cauchy stress tensor for the water constituent in terms of the chemical potential, μ^w, we take (Lai et al., 1991)

$$\nabla \cdot \boldsymbol{\sigma}^w = -c^w \nabla \mu^w. \tag{19}$$

Using the constitutive relations given by Eqs. 15, 18, and 19, together with the momentum equation for the mixture given by Eq. 7, provides the Gibbs–Duhem equation for the mixture under isothermal conditions (Tombs and Peacocke, 1974). Upon integration of the Gibbs–Duhem equation, the chemical potential for the water constituent is found to be

$$\mu^w = \mu_0^w + \frac{1}{c^w}\left(p - k_B T(c^+ + c^- + c^F)\right), \tag{20}$$

where the concentration of the solvent, c^w, is taken to be constant. Combining Eqs. 19 and 20 provides the constitutive equation for $\boldsymbol{\sigma}^w$ given by

$$\boldsymbol{\sigma}^w = \left(-p + k_B T(c^+ + c^- + c^F)\right)\mathbf{I}$$

$$\Rightarrow \nabla \cdot \boldsymbol{\sigma}^w = -\nabla p + k_B T \nabla (c^+ + c^- + c^F). \tag{21}$$

Reduced form of the equations

Combining the constitutive relationships given by Eqs. 15, 18, and 21 with the conservation equations given by Eqs. 3–5 provides the following reduced form of the momentum equations:

$$\frac{1}{k}(\mathbf{v}^s - \mathbf{v}^w) = \nabla \cdot \boldsymbol{\sigma}^E - k_B T \nabla c^F - nqc^F \mathbf{E}, \tag{22}$$

$$\frac{1}{k}(\mathbf{v}^s - \mathbf{v}^w) = \nabla p - k_B T \nabla (c^+ + c^- + c^F) - f_d^+ \mathbf{J}^+ - f_d^- \mathbf{J}^-$$

$$= \nabla p - k_B T \nabla c^F - q(\delta + nc^F)\mathbf{E}, \tag{23}$$

and

$$\mathbf{J}^\pm = -D^\pm \left(\nabla c^\pm - \frac{z^\pm q c^\pm}{k_B T} \mathbf{E} \right), \tag{24}$$

where we have introduced the diffusion coefficient, $D^\pm$, for the mobile ions by invoking the Stokes–Einstein equation, $D^\pm = k_B T / f_d^\pm$. Notice that, when Eqs. 22 and 23 are combined, Eq. 7 is obtained, which corresponds to the conservation of linear momentum for the mixture as a whole.

The equilibrium configuration

The expression for the flux of cations and anions given by Eq. 24 is identical to the electrochemical flux vectors used by Stace and Damiano (2001). In equilibrium, the flux of all constituents vanishes, and thus $\mathbf{J}^+ = \mathbf{J}^- = \mathbf{v}^s = \mathbf{v}^w = \mathbf{0}$. In this state, Eqs. 22–24 reduce to

$$\nabla \cdot \boldsymbol{\sigma}^E = k_B T \nabla c^F + nqc^F \mathbf{E}, \tag{25}$$

$$\nabla p = \nabla \cdot \boldsymbol{\sigma}^E + q\delta \mathbf{E} = k_B T \nabla (c^+ + c^- + c^F), \tag{26}$$

and

$$\mathbf{J}^\pm = \mathbf{0} \Rightarrow \nabla c^\pm = \frac{z^\pm q c^\pm}{k_B T} \mathbf{E}. \tag{27}$$

Using the definition of δ from Eq. 8, we note that Eqs. 26 and 27 combine to give Eq. 25. In the absence of an applied stress traction at the luminal glycocalyx boundary, Eqs. 25 and 27, together with Gauss's law (Eq. 13) and the definition of δ (Eq. 8), provide the closed system of equations necessary to determine the equilibrium configuration of the layer corresponding to a specified distribution for $c^F(\mathbf{x}, t_0)$. We shall choose this state as the prestressed reference configuration, where $\boldsymbol{\sigma}^E(\mathbf{x}, t_0)$ corresponds to the tensile stress distribution within the matrix in equilibrium. Under deformation of the layer, c^F becomes one of the unknown dependent variables.

Dimensional analysis of the governing equations

Using an asterisk to denote dimensionless variables, the independent and dependent variables are nondimensionalized as follows:

$$\mathbf{x} = R_0 \mathbf{x}^*, \quad \mathbf{X} = R_0 \mathbf{X}^*, \quad t = \tau_c t^*, \tag{28}$$

$$c^F = c_0^F c^{*F}, \quad c^\pm = c_0^+ c^{*\pm},$$

$$\delta = c_0^+ \delta^*, \quad \mathbf{E} = \frac{q R_0 c_0^+}{\epsilon} \mathbf{E}^*, \tag{29}$$

where c_0^+ is the concentration of mobile cations in the blood at the center of the capillary lumen. Henceforth, it will be assumed that $c_0^- = c_0^+$. We have taken the capillary radius, R_0, as our characteristic length scale and τ_c as a characteristic time scale to be assigned later. In addition, the dimensionless permeability, ion fluxes, extra-stress tensor, and osmotic pressure are defined as

$$k = k_0 k^*, \quad \mathbf{J}^\pm = \frac{c_0^+ D^\pm}{R_0} \mathbf{J}^{*\pm},$$

$$\boldsymbol{\sigma}^E = k_B T c_0^F \boldsymbol{\sigma}^{*E}, \quad p = k_B T c_0^+ p^*, \tag{30}$$

where k_0 is the solid-matrix permeability to water in the reference configuration. Using these definitions, the dimensionless equations governing Gauss's law and the equilibrium configuration are given respectively by

$$\nabla^* \cdot \mathbf{E}^* = \delta^* = z^+ c^{*+} + z^- c^{*-} - \xi_0 c^{*\mathrm{F}}, \quad (31)$$

$$\mathscr{F}\nabla^* \cdot \boldsymbol{\sigma}^{*\mathrm{E}} = \mathscr{F}\nabla^* c^{*\mathrm{F}} + \xi_0 Q c^{*\mathrm{F}} \mathbf{E}^*, \quad (32)$$

$$\nabla^* p^* = \mathscr{F}\nabla^* \cdot \boldsymbol{\sigma}^{*\mathrm{E}} + Q\delta^* \mathbf{E}^* = \nabla^*(c^{*+} + c^{*-} + \mathscr{F} c^{*\mathrm{F}}), \quad (33)$$

and

$$\mathbf{J}^{*\pm} = \mathbf{0} \Rightarrow \nabla^* c^{*\pm} = z^{\pm} Q c^{*\pm} \mathbf{E}^*. \quad (34)$$

The three dimensionless groups that arise are

$$\mathscr{F} \equiv \frac{c_0^{\mathrm{F}}}{c_0^+}, \quad \xi_0 \equiv n\mathscr{F} \equiv \frac{n c_0^{\mathrm{F}}}{c_0^+}, \quad Q \equiv \frac{q^2 R_0^2 c_0^+}{\epsilon k_{\mathrm{B}} T}, \quad (35)$$

where $\mathscr{F}$ denotes the ratio of glycocalyx concentration to cation concentration in blood, and ξ_0 denotes the ratio of glycocalyx fixed-charge density to the monovalent cationic charge density of blood. In aqueous solutions containing 0.14 M NaCl concentrations, such as normal saline or whole blood, $Q \approx 2 \times 10^8$ for a characteristic length scale associated with a 5-μm-diameter capillary.

The macromolecular concentrations of mucopolysaccharide structures devoid of collagen are typically low compared with the ion concentration of normal saline. Assuming this to be the case for the glycocalyx, and taking the mean valence, n, of the proteoglycan/glycoprotein/glycosaminoglycan aggregates of the layer to be large compared with unity, we assume that the dimensionless parameters are ordered such that $Q^{-1} \ll \mathscr{F} \ll \xi_0 \ll 1$.

According to the scaling rules defined above, $c^{*\pm} \sim O(1)$, $c^{*\mathrm{F}} \sim O(1)$, and $\nabla^* c^{*\mathrm{F}} \sim O(1)$. Furthermore, in equilibrium, it can be shown that local departures from electroneutrality are small such that $\delta^* \sim O(\xi_0/Q)$ (Stace and Damiano, 2001). We will later show that this assertion is consistent with the analysis that follows. From the dimensionless form of Gauss's law, given by the first of Eq. 31, we must then require that $\mathbf{E}^* = \nabla^* V^* \sim O(\xi_0/Q)$; and, although $z^+ c^{*+} \sim O(1)$ and $z^- c^{*-} \sim O(1)$, by the definition of δ^* given by the second of Eq. 31, we see that the sum of these two quantities is $O(\xi_0)$. That is,

$$\nabla^* \cdot \mathbf{E}^* = \delta^* \sim O(\xi_0/Q) \Rightarrow z^+ c^{*+} + z^- c^{*-} \approx \xi_0 c^{*\mathrm{F}} \sim O(\xi_0). \quad (36)$$

Using our result that $Q\mathbf{E}^* \sim O(\xi_0)$ in Eq. 32, we obtain

$$\mathscr{F}\nabla^* \cdot \boldsymbol{\sigma}^{*\mathrm{E}} \sim \mathscr{F}O(1) + \xi_0 O(\xi_0) \sim O(\mathscr{F} + \xi_0^2) \Rightarrow \nabla^* \cdot \boldsymbol{\sigma}^{*\mathrm{E}} \sim O(1 + \xi_0^2/\mathscr{F}) \sim O(1 + n^2\mathscr{F}). \quad (37)$$

If the equation associated with the cations in Eq. 34 is added to the equation associated with the anions, and the result of Eq. 36 is used, we obtain

$$\nabla^*(c^{*+} + c^{*-}) = (z^+ c^{*+} + z^- c^{*-}) Q\mathbf{E}^* \sim O(\xi_0^2). \quad (38)$$

Finally, using Eqs. 36 and 37 in Eq. 33, we obtain

$$O(\mathscr{F} + \xi_0^2) \sim \nabla^* p^* = \nabla^*(c^{*+} + c^{*-}) + O(\mathscr{F}), \quad (39)$$

which is consistent with Eq. 38 if the terms $O(\mathscr{F})$ on either side cancel, which they therefore must. From this we see the self consistency of the ordering we have given.

Axisymmetric equations for purely radial finite deformations of the glycocalyx

In Appendix A, the governing equations are written in the Eulerian cylindrical coordinates (r, θ, z) and then transformed into the Lagrangian cylindrical coordinates (R, Θ, Z) for the special case of purely radial axisymmetric deformations in the absence of axial flow. There it is shown that, under such conditions, the continuity equation and boundary conditions (see Appendix C for details) for the fluid constituent require that the radial fluid velocity component must also vanish.

In Eulerian variables, the momentum equation for the solid constituent (see Eq. A2) is defined on the unknown domain $a(t) \le r \le R_0$, where $a(t)$ is the instantaneous radial position of the glycocalyx interface with the plasma in the lumen, and $a_{\mathrm{o}} = a(t_0)$ is the value of a in the equilibrium configuration. When dealing with large deformations of the glycocalyx, it becomes more convenient to formulate the problem in material coordinates. In Appendix A, we develop the fully nonlinear mechano-electrochemical model of the glycocalyx that applies over the entire range of physiologically relevant radial deformations of the layer. Below, we summarize these one-dimensional equations but leave the details of their development to Appendix A.

Purely radial, axisymmetric, finite deformations of the layer, in which material points are displaced only along radial coordinate lines, constitute a principal state of strain. Under this loading configuration, the Lagrangian and Eulerian coordinates are related according to $r^*(R^*, t^*) = R^* + U_{\mathrm{R}}^*(R^*, t^*)$, $\theta = \Theta$, and $z^* = Z^*$ where U_{R}^* is the dimensionless radial displacement of the solid matrix and is the only nonvanishing component of the solid matrix displacement field. The principal stretch ratios are then given by $\lambda_{\mathrm{r}} = \partial r^*/\partial R^*$, $\lambda_\theta = r^*/R^*$, and $\lambda_{\mathrm{z}} = 1$. In dimensionless axisymmetric Lagrangian variables, for purely radial deformations, the dimensionless nonlinear diffusion equation and the ion mass conservation and flux equations are given, respectively, by

$$\left(\frac{R_0^2}{D_0^{\mathrm{F}}\tau_{\mathrm{c}}}\right)\frac{\lambda_{\mathrm{r}}}{k^*}\frac{\partial(R^*\lambda_\theta)}{\partial t^*} = \frac{\partial \sigma_{\mathrm{rr}}^{*\mathrm{E}}}{\partial R^*} + \frac{\lambda_{\mathrm{r}}}{\lambda_\theta}\frac{\sigma_{\mathrm{rr}}^{*\mathrm{E}} - \sigma_{\theta\theta}^{*\mathrm{E}}}{R^*} - \frac{\partial c^{*\mathrm{F}}}{\partial R^*} - nQ\lambda_{\mathrm{r}} c^{*\mathrm{F}} E_{\mathrm{r}}^* \quad \alpha_0 \le R^* \le 1 \quad (40)$$

and

$$\left(\frac{R_0^2}{D_0^{\pm}\tau_c}\right)\lambda_r\lambda_\theta\frac{\partial c^{*\pm}}{\partial t^*} = -\frac{1}{R^*}\frac{\partial}{\partial R^*}\left(R^*\lambda_\theta J_r^{*\pm}(R^*, t^*)\right)$$

$$0 \le R^* \le 1, \quad (41)$$

where

$$J_r^{*\pm}(R^*, t^*) = -\left(\frac{1}{\lambda_r}\frac{\partial c^{*\pm}}{\partial R^*} - z^{\pm}Qc^{*\pm}E_r^*\right)$$

$$0 \le R^* \le 1, \quad (42)$$

$$E_r^* = \frac{1}{R^*\lambda_\theta}\int_{R^*}^{1}\delta^*(\tilde{R}^*, t^*)\lambda_r\lambda_\theta\tilde{R}^*\,d\tilde{R}^*, \quad (43)$$

$$\delta^*(R^*, t^*) = z^+c^{*+}(R^*, t^*) + z^-c^{*-}(R^*, t^*) - \xi_0c^{*F}(R^*, t^*), \quad (44)$$

$$c^{*F} = \frac{f(R^*)}{\lambda_r\lambda_\theta}, \quad (45)$$

$\alpha_0 = a_0/R_0$, and $D_0^F = k_0k_BTc_0^F$. For the deformations considered here, the continuity equation for the solid matrix given by Eq. 11 reduces to Eq. 45 where $f(R^*)$ corresponds to the normalized shape of the glycocalyx concentration distribution in the reference configuration and $J = \det \mathbf{F} = \lambda_r\lambda_\theta$. In general, $f(R^*) = 0$ for $R^* < \alpha_0$, and increases sharply to a maximum of 1 for $R^* > \alpha_0$. For computational purposes, it will be taken to be a unit-step function, $f(R^*) = H(R^* - \alpha_0)$, but this is not assumed in the derivation of the equations that follow. The parameter D_0^F represents the effective Fickian diffusion coefficient, in the reference configuration, if the glycocalyx matrix were hydrated in a nonelectrolytic solution.

The pseudo-equilibrium approximation for monovalent ionic transport

Although physiologic deformations of the glycocalyx can typically be large, if $\mathcal{F} \ll \xi_0 \ll 1$, these deformations induce only small perturbations in the ion concentrations away from their initial equilibrium distributions at t_0. However, we shall not assume that the ion distributions, $c^{*+}(R^*, t^*)$ and $c^{*-}(R^*, t^*)$, remain equal to their initial equilibrium distributions, but rather that $c^{*+}(R^*, t^*)$ and $c^{*-}(R^*, t^*)$ change in such a way as to continuously correspond to the equilibrium distributions associated with each instantaneous glycocalyx distribution, $c^{*F}(R^*, t^*)$. This is equivalent to assuming that the transport of monovalent mobile ions occurs as a pseudo-equilibrium process. Significant simplifications in the analysis can be made by invoking this pseudo-equilibrium approximation because many of the relationships derived by Stace and Damiano (2001) for the case of static δ^* can be adapted to the problem with deformation. Physically, the motivation for this assumption lies in the realization that free unbalanced electric charges generate immense electrostatic forces that drive the system back to local charge neutrality very rapidly. Even small charge imbalances give rise to large electromotive forces. Furthermore, because the characteristic Fickian diffusion time, R_0^2/D^+, associated with the mobile ions is many orders of magnitude smaller than the characteristic Fickian diffusion time, R_0^2/D_0^F, associated with the glycocalyx molecules, the cations experience very little resistance to their motion through the solvent. Thus, strong electromotive forces combined with low ionic drag result in a rapid and continuous redistribution of ions into their instantaneous and nearly electroneutral equilibrium configurations.

We now establish this formally. Suppose we choose τ_c such that $\partial_{t^*}(R^*\lambda_\theta)$ on the left-hand side of Eq. 40 is $O(1)$. On the basis of Eq. 36, we make the assertion, which we will later show to be self-consistent, that the total variation in $c^{*\pm}$ is $O(\xi_0)$. Because the variation in $R^*\lambda_\theta$ is $O(1)$, the quantity $\partial_{t^*}c^{*\pm}/\partial_{t^*}(R^*\lambda_\theta)$ is $O(\xi_0)$, and, therefore, if we divide the left-hand side of Eq. 41 by the left-hand side of Eq. 40, we see that this ratio is $O(\xi_0D^F/D^{\pm})$, which is a very small quantity because $D^F \ll D^{\pm}$. We also note that τ_c cancels out of this ratio, so the choice of τ_c made above is not restrictive. However, the terms on the right-hand side of Eq. 40 are $O(1 + \xi_0^2/\mathcal{F})$, so the left-hand side must be $O(1 + \xi_0^2/\mathcal{F})$ or smaller. Therefore, if $\xi_0^2/\mathcal{F}$ is $O(1)$ or smaller, the left-hand side of Eq. 41 is $O(\xi_0D^F/D^{\pm})$ or smaller.

In contrast, the right-hand side of Eq. 41 is $O(\xi_0)$, and we have just established that the left-hand side is $O(\xi_0D^F/D^{\pm})$ or smaller, thus making it $O(D^F/D^{\pm})$ smaller than the right-hand side. (More precisely, the arguments made here lead to the same approximation even if $\xi_0^2/\mathcal{F} \gg 1$, as long as $(D^F/D^{\pm})$ $(\xi_0^2/\mathcal{F}) \ll 1$.) We therefore neglect the left-hand side in comparison to the right-hand side and set the latter to zero, from which we conclude that $R^*\lambda_\theta J_r^{*\pm}(R^*, t^*)$ is spatially uniform, and, further, that the ionic flux, $J_r^{*\pm}$, must vanish identically to match the zero-flux boundary condition at $R^* = 1$ (see Appendix C).

Invoking this approximation, we assume that, during deformation of the glycocalyx, departures from the equilibrium ion distributions are so slight, and ionic transport is so fast, that the ions establish equilibrium instantaneously at every instant in time. Henceforth, we shall refer to this as the pseudo-equilibrium approximation for ionic transport. As we shall see, appropriately modified versions of the

equilibrium distributions given by Stace and Damiano (2001) provide reasonable approximations for $c^{*\pm}(R^*, t^*)$ and $\delta^*(R^*, t^*)$. Having shown that the pseudo-equilibrium approximation is valid independent of the choice of τ_c, we are at liberty to choose τ_c arbitrarily. A convenient choice for computational purposes is to take $\tau_c = R_0^2(D^+D_0^F)^{-1/2} = R_0^2(D^+k_0k_BTc_0^F)^{-1/2}$.

Analytic implications of the pseudo-equilibrium approximation

In equilibrium, the flux of all diffusing species vanishes, and one can show (Stace and Damiano, 2001) that, in the reference configuration (i.e., when $r^* = R^*$, $\lambda_r = \lambda_\theta = 1$), the equilibrium distributions associated with the mobile ions are related according to $c^{*+}(R^*, t_0^*) = 1/c^{*-}(R^*, t_0^*)$. Based on the dimensional considerations stated above, we impose the pseudo-equilibrium approximation on the transport of mobile ions such that the above result for the ion concentrations applies instantaneously for all values of t^*, not just in the reference configuration. This is equivalent to saying that, for a given instantaneous deformed configuration of the glycocalyx, the associated instantaneous ion distributions are identical to the equilibrium ion distributions that would correspond to that deformation. Invoking the pseudo-equilibrium approximation, we assert that

$$c^{*+}(R^*, t^*) \approx \frac{1}{c^{*-}(R^*, t^*)}. \tag{46}$$

Because $\delta^* \sim O(\xi_0/Q)$, from Eq. 44 we have

$$z^+c^{*+}(R^*, t^*) + z^-c^{*-}(R^*, t^*) - \xi_0 c^{*F}(R^*, t^*) \approx 0 \tag{47}$$

for all values of R^* and t^*. This is consistent with the quasi-static approximation for δ^* made by Stace and Damiano (2001) and with the pseudo-equilibrium approximation made here, because physiological deformations of the glycocalyx result in only slight perturbations in the equilibrium distributions of $c^{*\pm}$ and δ^*. Substituting for c^{*-} from Eq. 46 provides a quadratic equation in c^{*+} in terms of c^{*F}, which has the solution

$$\begin{aligned} c^{*+}(R^*, t^*) &\approx \frac{1}{2}\left(\xi_0 c^{*F}(R^*, t^*) + \sqrt{(\xi_0 c^{*F}(R^*, t^*))^2 + 4}\right) \\ &= \frac{1}{2}\left(\frac{\xi_0 f(R^*)}{\lambda_r\lambda_\theta} + \sqrt{\left(\frac{\xi_0 f(R^*)}{\lambda_r\lambda_\theta}\right)^2 + 4}\right), \end{aligned} \tag{48}$$

where we have used Eq. 45 for c^{*F}. Consistent with our assertion made earlier, it is evident from Eq. 48 that, while c^{*+} is $O(1)$, spatiotemporal variations in c^{*+} are $O(\xi_0)$.

By the pseudo-equilibrium approximation, we set Eq. 42 equal to zero, multiply the resulting equation for the cationic constituent by $R^*\lambda_\theta/c^{*+}$ and differentiate with respect to R^* to obtain

$$\frac{\partial}{\partial R^*}\left(\frac{\lambda_\theta}{\lambda_r}\frac{R^*}{c^{*+}}\frac{\partial c^{*+}}{\partial R^*}\right) - z^+Q\frac{\partial}{\partial R^*}(R^*\lambda_\theta E_r^*) = 0. \tag{49}$$

However, from Gauss's law, given in reference coordinates by Eq. 43, we note that

$$\frac{\partial}{\partial R^*}(R^*\lambda_\theta E_r^*) = R^*\lambda_r\lambda_\theta\delta^*, \tag{50}$$

which, when combined with the previous result, provides an expression for δ^* in terms of the principal stretch ratios, λ_r and λ_θ, given by

$$\delta^*(R^*, t^*) \approx \frac{1}{z^+Q\lambda_r\lambda_\theta R^*}\frac{\partial}{\partial R^*}\left(\frac{\lambda_\theta}{\lambda_r}R^*\frac{\partial}{\partial R^*}(\ln c^{*+})\right), \tag{51}$$

where, if $z^+ = -z^- = 1$, c^{*+} is given by Eq. 48. Recalling from Eq. 48 that spatial variations in c^{*+} are $O(\xi_0)$, Eq. 51 verifies our assertion made earlier on dimensional grounds that in pseudo-equilibrium, $\delta^* \sim O(\xi_0/Q)$.

Using Eqs. 48, 50, and 51, and noting that in Lagrangian variables

$$E_r^*(R^*) = -\frac{1}{\lambda_r}\frac{\partial V^*}{\partial R^*}, \tag{52}$$

then, according to the pseudo-equilibrium approximation, the voltage is given by

$$\begin{aligned} V^*(R^*) &\approx -\frac{1}{z^+Q}\ln(c^{*+}(R^*)) \\ &\approx -\frac{1}{Q}\ln\left(\frac{1}{2}\left[\frac{\xi_0 f(R^*)}{\lambda_r\lambda_\theta} + \sqrt{\left(\frac{\xi_0 f(R^*)}{\lambda_r\lambda_\theta}\right)^2 + 4}\right]\right), \end{aligned} \tag{53}$$

where we have taken the reference voltage in the center of the vessel lumen to be zero. Note that the first of Eq. 53 is valid for arbitrary cation valence, whereas the second assumes monovalent cations. Once again, Eq. 53 is seen to be consistent with our assertion that $E_r^* = -\partial V^*/\partial R^* \sim O(\xi_0/Q)$.

Note that, in the equilibrium configuration, $\lambda_r(R^*, t_0^*) = \lambda_\theta(R^*, t_0^*) = 1$ and $r^* = R^*$, and Eqs. 48, 51, and 53 reduce to the steady-state distributions predicted by the electrochemical model of Stace and Damiano (2001). Thus, these

results generalize the steady-state expressions to account for deformations of the glycocalyx, wherein ion transport satisfies the pseudo-equilibrium approximation described above.

Using Eq. 51 to evaluate the integral in Eq. 43, the nonlinear diffusion equation governing glycocalyx deformation given by Eq. 40 reduces to

$$\sqrt{\frac{D^+}{D_0^{\mathrm{F}}}}\frac{\lambda_{\mathrm{r}}}{k^*}\frac{\partial(R^*\lambda_\theta)}{\partial t^*}=\frac{\partial\sigma_{\mathrm{rr}}^{*\mathrm{E}}}{\partial R^*}+\frac{\lambda_{\mathrm{r}}}{\lambda_\theta}\frac{\sigma_{\mathrm{rr}}^{*\mathrm{E}}-\sigma_{\theta\theta}^{*\mathrm{E}}}{R^*}-\frac{\partial}{\partial R^*}\left(\frac{f(R^*)}{\lambda_{\mathrm{r}}\lambda_\theta}\right)-\frac{n}{z^+}\frac{f(R^*)}{\lambda_{\mathrm{r}}\lambda_\theta}\frac{\partial}{\partial R^*}(\ln c^{*+})\qquad \alpha_0\le R^*\le 1, \quad (54)$$

where c^{*+} is given by Eq. 48. Thus, the pseudo-equilibrium approximation for ionic transport reduces the coupled system of three nonlinear, partial integro-differential equations (Eqs. 40 and 41) to two algebraic equations for c^{*+} and c^{*-} (Eqs. 46 and 48) and one nonlinear partial differential equation (Eq. 54).

Reduced nonlinear diffusion equation

All that remains to establish closure for the model is to specify the strain-dependent constitutive relationships for the glycocalyx permeability, k^*, and elastic stress components, $\sigma_{\mathrm{rr}}^{*\mathrm{E}}$ and $\sigma_{\theta\theta}^{*\mathrm{E}}$. The details of this are left to Appendix B. Using these constitutive relationships (see Eqs. B1 and B4), the stress components and permeability are expressed in terms of the principal stretch ratios, λ_{r} and λ_θ. Substitution of these relations into Eq. 54 and defining the dimensionless prestress $T_0^* = T_0/k_{\mathrm{B}}Tc_0^{\mathrm{F}}$, the dimensionless nonlinear diffusion equation reduces to the second-order, nonlinear, partial differential equation in the principal stretch ratio, λ_θ, given by

$$\sqrt{\frac{D^+}{D_0^{\mathrm{F}}}}\frac{\lambda_{\mathrm{r}}}{k^*}\frac{\partial(R^*\lambda_\theta)}{\partial t^*}=\frac{T_0^*(R^*)}{R^*}\left(\frac{\lambda_{\mathrm{r}}^2}{\lambda_\theta^2}-1\right)+\frac{\partial}{\partial R^*}\left(T_0^*(R^*)\frac{\lambda_{\mathrm{r}}}{\lambda_\theta}-\frac{f(R^*)}{\lambda_{\mathrm{r}}\lambda_\theta}\right)-\frac{n}{z^+}\frac{f(R^*)}{\lambda_{\mathrm{r}}\lambda_\theta}\frac{\partial}{\partial R^*}(\ln c^{*+})\qquad \alpha_0\le R^*\le 1, \quad (55)$$

where $\lambda_{\mathrm{r}} = \partial(R^*\lambda_\theta)/\partial R^*$, c^{*+} is given by Eq. 48, and $k^* = k/k_0$ is given by Eq. B1. The dimensionless quantities that define the parameter space for the model are then given by α_0, D_0^{F}/D^+, M, ξ_0, and $\mathcal{F}$ (or $n = \xi_0/\mathcal{F}$).

Note that, in terms of the dimensionless chemical potential functions, $\mu^{*+} = \mu^+/(k_{\mathrm{B}}T)$ for the cations and $\mu^{*\mathrm{s}} = \mu^{\mathrm{s}}/(k_{\mathrm{B}}T)$ for the glycocalyx matrix, Eq. 55 can be written as

$$\sqrt{\frac{D^+}{D_0^{\mathrm{F}}}}\frac{\lambda_{\mathrm{r}}}{k^*}\frac{\partial(R^*\lambda_\theta)}{\partial t^*}=\frac{T_0^*(R^*)}{R^*}\left(\frac{\lambda_{\mathrm{r}}^2}{\lambda_\theta^2}-1\right)+\frac{\partial}{\partial R^*}\left(T_0^*(R^*)\frac{\lambda_{\mathrm{r}}}{\lambda_\theta}\right)-\frac{f(R^*)}{\lambda_{\mathrm{r}}\lambda_\theta}\frac{\partial}{\partial R^*}\left(\mu^{*\mathrm{s}}+\frac{n}{z^+}\mu^{*+}\right)\qquad \alpha_0\le R^*\le 1. \quad (56)$$

Thus we see that, by the pseudo-equilibrium approximation, the electrostatic potential of the glycocalyx matrix is locally and instantaneously equal to n/z^+ times the chemical potential of the cations. It is convenient to introduce the electrochemical potential, $\mu_{\mathrm{ec}}^{*\mathrm{s}}$, of the matrix, where

$$\frac{\partial\mu_{\mathrm{ec}}^{*\mathrm{s}}}{\partial R^*}\equiv\frac{\partial}{\partial R^*}\left(\mu^{*\mathrm{s}}+\frac{n}{z^+}\mu^{*+}\right)=\frac{\partial}{\partial R^*}\left(\ln c^{*\mathrm{F}}+\frac{n}{z^+}\ln c^{*+}\right)=\frac{\partial}{\partial R^*}\ln(c^{*\mathrm{F}}(c^{*+})^{\mathrm{n}/z^+}), \quad (57)$$

and $c^{*\mathrm{F}}$ and c^{*+} are given in terms of the principal stretch ratios by Eqs. 45 and 48, respectively. From Eq. 57, it is evident that if $n \gg z^+$, then even a small perturbation in the chemical potential of the cations can be accompanied by a large electrochemical flux of the glycocalyx.

In Eq. 56, the first three terms on the right-hand side are associated with the divergence of the stress tensor, $\boldsymbol{\sigma}^{*\mathrm{E}}$, of the glycocalyx solid matrix. Because the constitutive equation that was invoked for $\boldsymbol{\sigma}^{*\mathrm{E}}$ assumed that the glycocalyx can only support tension, then, under compression, the total contribution from these terms diminishes (with the exception of the hoop stress associated with the second term on the right-hand side of Eq. 56). Alternatively, the last two terms on the right-hand side of Eq. 56, which we have identified as the product of $c^{*\mathrm{F}}$ and the gradient in the electrochemical potential given by Eq. 57, increase with increasing compression. The left-hand side represents the local permeation-induced drag associated with the motion of the solid matrix through the plasma. During recovery of the compressed matrix into plasma, this drag force resists the restoring force associated with $\nabla^*\mu_{\mathrm{ec}}^{*\mathrm{s}}$. As equilibrium is approached, tension in the matrix increases while the drag force and $c^{*\mathrm{F}}\nabla^*\mu_{\mathrm{ec}}^{*\mathrm{s}}$ decrease until a new balance is achieved between the isotropic tension in the matrix, associated with $\nabla^*\cdot\boldsymbol{\sigma}^{*\mathrm{E}}$, and the gradient in the electrochemical potential, $\nabla^*\mu_{\mathrm{ec}}^{*\mathrm{s}}$.

Determination of $T_0^*(R^*)$ from the equilibrium configuration

The distribution, $T_0^*(R^*)$, appearing in Eq. 55 still remains to be determined. In equilibrium, a state of tension sets up in the matrix that balances the electrochemical forces in the glycocalyx and gives rise to a static electric field and nonuniform distributions in the concentrations of mobile ions. This tension is given by the function $T_0^*(R^*)$ and is determined by considering the equilibrium configuration of the glycocalyx when the left-hand side of Eq. 55 vanishes and $\lambda_r = \lambda_\theta = 1$. Integrating the resulting equilibrium equation by parts, we obtain

$$T_0^*(R^*) = f(R^*) - \frac{1}{\mathcal{F}}\left(2 - \sqrt{\xi_0^2 f^2(R^*) + 4}\right). \quad (58)$$

Using Eq. 58 on the right-hand side of Eq. 55 provides a closed model for the displacement field of the glycocalyx subject to boundary conditions prescribed at $R^* = \alpha_0$ and $R^* = 1$.

Boundary conditions under the pseudo-equilibrium approximation

The general form of the boundary conditions for the axisymmetric one-dimensional deformations considered here are given in Eulerian variables in Appendix C. However, significant simplifications to some of these conditions can be made by invoking the pseudo-equilibrium approximation. In Lagrangian variables, the axisymmetric conditions are given by

$$\left.\frac{\partial c^{*\pm}}{\partial R^*}\right|_{R^*=0} = 0$$

and

$$E_r^*(R^* = 0, t^*) = -\left.\frac{\partial V^*}{\partial R^*}\right|_{R^*=0} = 0, \quad (59)$$

and the condition for global charge neutrality is given by

$$E_r^*(R^* = 1, t^*) = -\left.\frac{\partial V^*}{\partial R^*}\right|_{R^*=1} = 0. \quad (60)$$

Using Eqs. 42 and 60, the zero-flux boundary condition at the endothelial cell wall is given by

$$J_r^{*\pm}(R^* = 1, t^*) = \frac{1}{\lambda_r}\left.\frac{\partial c^{*\pm}}{\partial R^*}\right|_{R^*=1} - z^{\pm}Qc^{*\pm}E_r^*(R^* = 1, t^*) = 0$$

$$\Rightarrow \left.\frac{\partial c^{*\pm}}{\partial R^*}\right|_{R^*=1} = 0. \quad (61)$$

In terms of the principal stretch ratio, λ_θ, the boundary condition on the displacement field at the endothelial cell wall is

$$U_R^*(R^* = 1, t^*) = 0 \Rightarrow \lambda_\theta(R^* = 1, t^*) = 1. \quad (62)$$

All of the boundary and symmetry conditions stated above are independent of the pseudo-equilibrium approximation. However, invoking the pseudo-equilibrium approximation greatly simplifies the interfacial boundary conditions (see Eqs. C2 to C4). Substituting the first of Eq. 48 into Eq. 49, we note that

$$Z^+Q\lambda_r E_r^* = \frac{\partial}{\partial R^*}(\ln c^{*+}) = \frac{\xi_0 \partial c^{*F}/\partial R^*}{\sqrt{(\xi_0 c^{*F}(R^*, t^*))^2 + 4}}. \quad (63)$$

Using this result, the integral term that appears in the interfacial condition associated with the momentum equation for the solid matrix (see Eq. C2) can be expressed in dimensionless Lagrangian variables and integrated as

$$\begin{aligned} Z^+Q &\int_{\alpha^-(t)}^{\alpha^+(t)} c^{*F}(r^*, t^*)E_r^*(r^*, t^*)\,dr^* \\ &= Z^+Q\int_{\alpha_0^-}^{\alpha_0^+} c^{*F}(R^*, t^*)E_r^*(R^*, t^*)\lambda_r\,dR^* \\ &= \xi_0\int_{\alpha_0^-}^{\alpha_0^+} \frac{c^{*F}\partial c^{*F}/\partial R^*}{\sqrt{(\xi_0 c^{*F})^2 + 4}}\,dR^* \\ &= \frac{1}{\xi_0}\left\{\sqrt{(\xi_0 c^{*F}(\alpha_0^+, t^*))^2 + 4} - \sqrt{(\xi_0 c^{*F}(\alpha_0^-, t^*))^2 + 4}\right\} \\ &= \frac{1}{\xi_0}\left[\!\left[\sqrt{(\xi_0 c^{*F}(R^*, t^*))^2 + 4}\right]\!\right], \end{aligned} \quad (64)$$

where we define the jump in a quantity $\phi(R, t)$ across $\Gamma(t)$ as being $[\![\phi]\!] \equiv \phi(\alpha_0^+) - \phi(\alpha_0^-)$. Because there is no solid matrix on the luminal side of the interface, $f(\alpha^-(t)) = f(\alpha_0^-) = 0$. Using this and Eq. 45, Eq. 64 becomes

$$\begin{aligned} Z^+Q &\int_{\alpha^-(t)}^{\alpha^+(t)} c^{*F}(r^*, t^*)E_r^*(r^*, t^*)\,dr^* \\ &= \frac{1}{\xi_0}\left\{\sqrt{\left(\frac{\xi_0 f(\alpha_0^+)}{\lambda_r(\alpha_0, t^*)\lambda_\theta(\alpha_0, t^*)}\right)^2 + 4} - 2\right\}. \end{aligned} \quad (65)$$

Thus, under the pseudo-equilibrium approximation, the interfacial boundary condition reduces to

$$t^*_{\mathrm{ext}}(t^*) = \left[\!\!\left[-T^*_0(R^*)\,\frac{\lambda_r}{\lambda_\theta} + \frac{f(R^*)}{\lambda_r\lambda_\theta} + \frac{n}{z^+\xi_0}\sqrt{\left(\frac{\xi_0 f(R^*)}{\lambda_r\lambda_\theta}\right)^2 + 4}\,\right]\!\!\right], \quad (66)$$

where $t^*_{\mathrm{ext}}(t^*)$ simulates the dimensionless radial normal component of the stress–traction exerted on the luminal interface of the layer by a passing leukocyte (see Appendix C). By definition, the distributions $T^*_0(R^*)$ and $f(R^*)$ vanish identically for $R^* \le \alpha_0^-$, and thus the terms that contain these quantities in Eq. 66 contribute nothing at $R^* = \alpha_0^-$. Taking $z^+ = 1$ and recalling that $\xi_0/n = \mathcal{F}$, we obtain the implicit nonlinear boundary condition at $R^* = \alpha_0$ given by

$$t^*_{\mathrm{ext}}(t^*) = -T^*_0(\alpha_0)\,\frac{\lambda_r(\alpha_0, t^*)}{\lambda_\theta(\alpha_0, t^*)} + \frac{f(\alpha_0)}{\lambda_r(\alpha_0, t^*)\lambda_\theta(\alpha_0, t^*)} + \frac{1}{\mathcal{F}}\left\{\sqrt{\left(\frac{\xi_0 f(\alpha_0)}{\lambda_r(\alpha_0, t^*)\lambda_\theta(\alpha_0, t^*)}\right)^2 + 4} - 2\right\}. \quad (67)$$

In the equilibrium configuration, $\lambda_r = \lambda_\theta = 1$, $t^*_{\mathrm{ext}} = 0$, and Eq. 67 reduces to

$$T^*_0(\alpha_0) = f(\alpha_0) + \frac{1}{\mathcal{F}}\left(\sqrt{\xi_0^2 f^2(\alpha_0) + 4} - 2\right), \quad (68)$$

which corresponds to Eq. 58 evaluated at $R^* = \alpha_0$. Thus the boundary and initial conditions are mutually consistent.

LINEARIZED ANALYSIS

Through a linearized analysis of the governing partial differential equation (PDE), given by Eq. 55, we investigate the behavior of the model as a function of the two most important parameters, the relative glycocalyx concentration, $\mathcal{F} \equiv c_0^{\mathrm{F}}/c_0^+$, and the relative glycocalyx fixed-charge density, $\xi_0 \equiv nc_0^{\mathrm{F}}/c_0^+ = n\mathcal{F}$. Of less importance are the parameters α_0 and M and the applied stress, $t^*_{\mathrm{ext}}(t^*)$. The analysis results in a closed-form asymptotic solution for the recovery time of the layer after compression that depends on ξ_0, $\mathcal{F}$, and α_0, but not on M. The dependence of the recovery time on M and large values of t^*_{ext} requires numerical solution of the nonlinear PDE.

In the remainder of this section, quantities are dimensionless unless otherwise stated, however the asterisk will be omitted for brevity, and we will take $f(R) = H(R - \alpha_0)$. Defining the quantity $\Delta\lambda(R, t) \equiv \lambda_\theta(R, t) - 1$, we assume that $\Delta\lambda \ll 1$ and expand the right-hand side of Eq. 55 in powers of $\Delta\lambda$, keeping only the lowest order terms. This assumption is reasonable for a thin glycocalyx, because Eq. A8 implies that if $\frac{1}{2} < \alpha_0 < 1$, then $1 \le \lambda_\theta \le \alpha_0^{-1}$, and therefore $0 \le \Delta\lambda \le (1 - \alpha_0)/\alpha_0 < 1$. This condition holds if the glycocalyx thickness is less than half of the capillary radius. In capillaries of mammalian skeletal muscle, α_0 is reported as ranging between 0.8 and 0.9 and therefore $\Delta\lambda < 0.25$ (Vink and Duling, 1996, 2000). For small strains, where $\Delta\lambda$ is considerably less than its upper bound, we equate terms in the power series expansion of Eq. 55 that are linear in $\Delta\lambda$ to obtain the linearized PDE given by

$$\sqrt{\frac{D^+}{D_0^{\mathrm{F}}}}\,\frac{\partial(\Delta\lambda)}{\partial t} = \frac{2}{\mathcal{F}}\left(\mathcal{F} - 1 + \frac{2 + \xi_0^2}{\sqrt{4 + \xi_0^2}}\right)\left(\frac{3}{R}\,\frac{\partial(\Delta\lambda)}{\partial R} + \frac{\partial^2(\Delta\lambda)}{\partial R^2}\right). \quad (69)$$

To obtain a solution for the recovery time of the layer in the absence of an externally applied stress (corresponding to the recovery of the glycocalyx into cell-free plasma), we linearize the boundary condition given by Eq. 67 and take $t_{\mathrm{ext}} = 0$. To derive a result for the steady-state strain, in contrast, we will retain t_{ext} but set the time derivative in Eq. 69 to zero.

The steady-state distribution can be determined analytically from Eq. 69 and the maximum strain at steady state (for dimensional σ_{ext}) is given to first order in $(1 - \alpha_0) \approx 0.2 \ll 1$ by

$$\Delta\lambda(\alpha_0) \approx \left(\frac{\sigma_{\mathrm{ext}}}{k_{\mathrm{B}}Tc_0^+}\right)\frac{(1 - \alpha_0)}{\left(2\mathcal{F} + \frac{3}{4}\,\xi_0^2\right)}. \quad (70)$$

Separation of variables results in an eigenvalue problem that can be used to determine the unsteady behavior of Eq. 69. The first nonzero eigenvalue determines the slowest characteristic time of the problem, and therefore the time scale for recovery. The mathematical details of the analysis are left to Appendix D. The spatial equation resulting from the eigenvalue problem may be solved exactly in terms of Bessel functions, however the resulting characteristic equation does not admit analytic expressions for the eigenvalues. We are able to find a closed-form estimate of the first nonzero eigenvalue though, by expanding the characteristic equation in a Taylor series and then analytically finding the positive root of the resulting polynomial. We use this approximate expression for the first nonzero eigenvalue to determine the slowest characteristic time of the problem, and we find that a good estimate for the 90% recovery time is given by the dimensional expression

$$\tau_1 \approx \frac{\ln(10)}{(6 - \sqrt{12})}\left(\frac{R_0^2}{k_0 k_{\mathrm{B}}Tc_0^+}\right)\frac{(1 - \alpha_0)^2}{(2\mathcal{F} + \frac{3}{4}\,\xi_0^2)}. \quad (71)$$

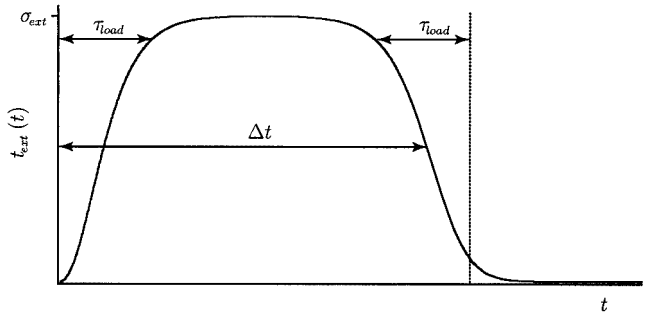

FIGURE 1 Time course of the magnitude, $t_{ext}(t)$, of the applied stress traction vector used to model the time-dependent loading of a leukocyte.

This formula predicts that, if $\xi_0^2 \ll \mathcal{F}$, then the recovery time is nearly independent of ξ_0, whereas for $\xi_0^2 \gg \mathcal{F}$, the recovery time varies in proportion to $1/\xi_0^2$. It also predicts that, for a very thin layer, when $1 - \alpha_0 \ll 1$, the recovery time varies quadratically with the dimensionless thickness, $1 - \alpha_0$. Notice that both $\Delta\lambda(\alpha_0)$ and τ_1 vary inversely with the same quantity, $2\mathcal{F} + \frac{3}{4}\xi_0^2$, and so the ratio of τ_1 to $\Delta\lambda(\alpha_0)$,

$$\frac{\tau_1}{\Delta\lambda(\alpha_0)} \approx \frac{\ln(10)}{(6 - \sqrt{12})}\left(\frac{R_0^2}{k_0\sigma_{ext}}\right)(1 - \alpha_0), \qquad (72)$$

is independent of ξ_0 and $\mathcal{F}$.

NUMERICAL METHODS

The nonlinear PDE given by Eq. 55 is also solved using a finite difference method and the numerical PDE-solving routine built in to Mathematica. The interfacial boundary condition given by Eq. 67 requires that we specify the time course of the external stress–traction vector used to simulate the stress imparted by a passing leukocyte. We assume the temporal dependence,

$$t_{ext}(t) = \sigma_{ext}\left(\frac{1}{2}\tanh\left(\frac{t}{\tau_{load}}\right)\left[\tanh\left(\frac{\Delta t - t}{\tau_{load}}\right) + 1\right]\right)^2, \quad (73)$$

where τ_{load} is the characteristic time associated with the loading rate, and Δt is the time interval over which the load is maintained. At $t = 0$, the load is zero but immediately starts rising, quadratically at first, and then exponentially as it approaches σ_{ext}. At $t \approx \Delta t$, the applied load drops exponentially to zero. This is shown schematically in Fig. 1.

After numerically solving Eq. 55, the 90% recovery time, τ, is calculated from the numerical solution. It is defined as the elapsed time from the initiation of unloading to the time at which $\lambda_\theta(\alpha_0, t)$ has returned to 10% of its maximum excursion from unity. That is, τ is the positive time that satisfies the relationship

$$\frac{\lambda_\theta(\alpha_0, \Delta t + \tau) - 1}{\max(\lambda_\theta(\alpha_0, t)) - 1} = 0.1. \qquad (74)$$

If the characteristic time, τ_{load}, associated with the loading and unloading rate is relatively long, there is sufficient time for the disturbance to diffuse throughout the glycocalyx such that the concentration distribution, $c^F(R, t)$, differs from the initial concentration distribution, $c^F(R, t_0)$, by only a time-dependent scalar multiple at each time, t, i.e., $c^F(R, t) \approx \psi(t)c^F(R, t_0)$. The recovery time, in this case, would not be limited by the material properties of the layer. However, if τ_{load} corresponds to a relatively short time, the permeability and restoring forces of the glycocalyx limit the rate of recovery. For a leukocyte 8–10-μm-long traveling at a 50–200 μm/s, the range in the unloading time would typically be $0.02 < \tau_{load} < 0.1$ s. Recalling that the recovery time of the glycocalyx in the wake of a passing leukocyte was reported by Vink et al. (1999) to be on the order of 1 s, we use a value of τ_{load}, which is much smaller than τ so that the recovery time is nearly independent of the unloading rate. This is balanced by the requirement that the PDE solver be able to obtain a numerical solution at high loading rates. Therefore, we typically take $\tau_{load} \lesssim \tau/30$.

RESULTS

In this section, results of the finite-difference implementation and asymptotic analyses are presented and compared. Invoking the pseudo-equilibrium approximation, the reduced nonlinear diffusion equation given by Eq. 55 is solved numerically using a finite difference method. As long as the pseudo-equilibrium approximation remains reasonable, the finite difference solution is capable of handling nonlinearities associated with arbitrarily large glycocalyx deformations, the interfacial boundary condition given by Eq. 67, and the strain-dependent permeability given by Eq. 93. Results of the finite difference solution are shown below for the response dynamics of the layer during radial compression and recovery. The dependence on problem parameters of the layer's recovery time into cell-free plasma is explored, and a comparison between numerical and analytical results is made. Finally, nonlinearities associated with loading rate, and the hysteresis that accompanies various loading cycles, are presented and compared with the static loading curves predicted by the linear and nonlinear theories.

Glycocalyx response dynamics in compression and recovery

The finite difference solution to Eq. 55 was obtained for λ_θ subject to the boundary condition at $R^* = 1$, given by the

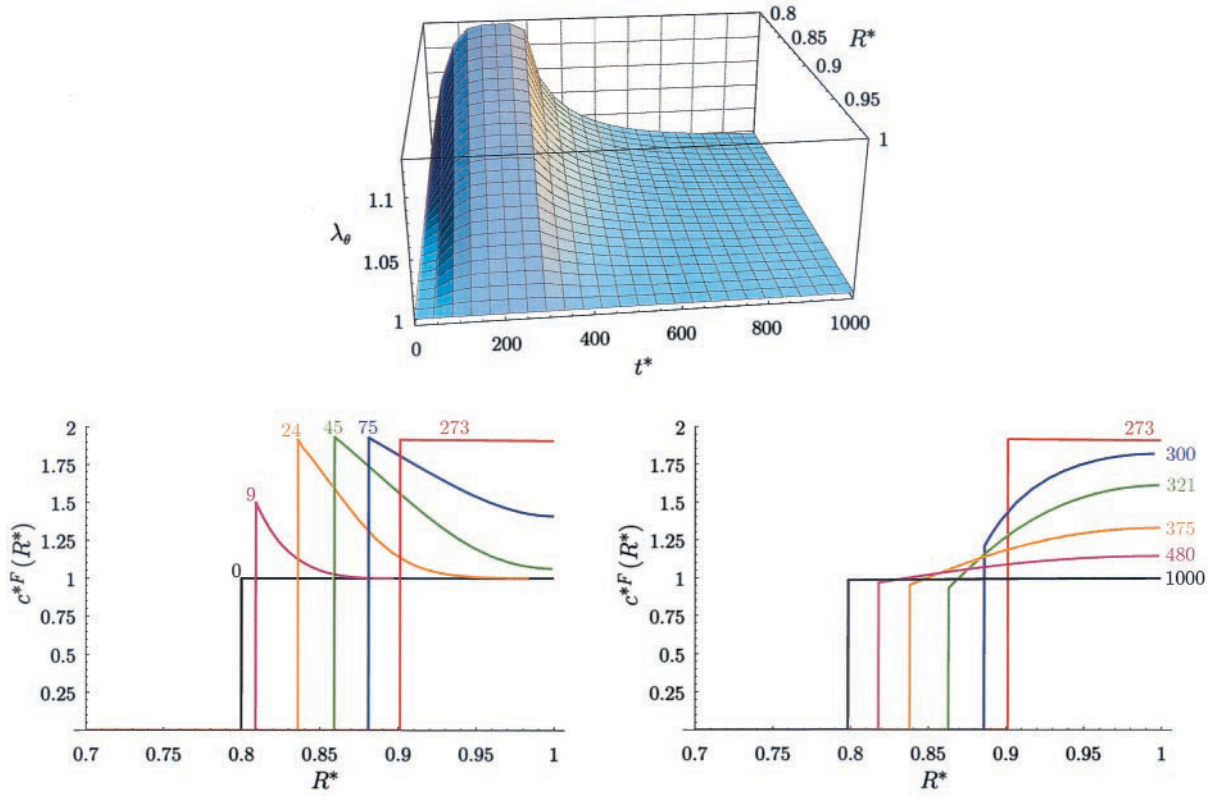

FIGURE 2 Three-dimensional plot (*top*) of the displacement field over space and time for $\mathcal{F} = 10^{-7}$, $\xi_0 = 0.01$, and $M = 0$. Glycocalyx concentration over space for different times (as indicated beside each curve) during compression (*bottom left*) and recovery (*bottom right*). The compressing load was applied in a time $\tau_{load} = 10$, which is more than 20 times faster than either the compression or recovery times. All times are in units of $\sqrt{\mathcal{F}}\tau_c = R_0^2/(k_0 k_B T c_0^+)(= 1.79 \times 10^{-3}$ s for $R_0 = 2.5$ μm, $k_0 = 10^{-11}$ cm^4(dyn-s)$^{-1}$, and $c_0^+ = 0.14$ M). Equation 53 reveals that, if $\xi_0 \ll 1$, the local glycocalyx concentration, $c^{*F}(R^*, t^*)$, is directly proportional to the local voltage potential, $V^*(R^*, t^*)$, and thus the instantaneous concentration distributions shown in the bottom two panels correspond to the instantaneous voltage distributions if the vertical axis is scaled by the factor $1/2k_BT\xi_0/q = 0.129$ mV, i.e., at equilibrium, the glycocalyx is 0.129 mV above the lumen if $\xi_0 = 0.01$.

second of Eq. 62, and the interfacial boundary condition given by Eq. 67. Figures 2 and 3 show results of this numerical solution for λ_θ as a function of space and time. Also shown are instantaneous glycocalyx concentration distributions at a number of times during compression and recovery. These distributions are obtained from Eq. A14 using the finite difference solution for λ_θ.

The concentration distributions of the glycocalyx in compression and recovery take on expected profiles. In the early stages of compression, the concentration distribution is elevated near the interface at which the external stress traction is applied, and falls off near the endothelium. As time progresses, the layer becomes thinner but more concentrated and eventually reaches a state of maximum compression with a concentration distribution that is nearly uniform over the entire thickness of the layer. In recovery, approximately the reverse is true; the concentration is lowest at the luminal interface and rises toward the endothelium. For a brief period of time, the local glycocalyx concentration near the interface can be lower than its steady-state value in the equilibrium configuration.

Recovery time

When the pseudo-equilibrium approximation is reasonable, the recovery time depends upon the material parameters ξ_0, $\mathcal{F}$, M, α_0, and k_0. However, because the recovery time varies in inverse proportion to the permeability parameter, k_0, results are more generally expressed in terms of the dimensionless recovery time, which is independent of k_0. The dimensional recovery time is shown on the right-hand axis of Fig. 4, corresponding to a matrix permeability of $k_0 = 10^{-11}$ cm^4(dyn-s)$^{-1}$. This value of k_0 was taken from estimates by Feng and Weinbaum (2000), which were inferred from a fiber matrix model based on the Brinkman equation. In what follows, the dependence of the dimensionless recovery time on the parameters ξ_0, $\mathcal{F}$, M, and α_0 will be examined.

Dependence on ξ_0 and $\mathcal{F}$

The parameters $\mathcal{F}$ and ξ_0 are the most physically significant in determining the recovery time of the glycocalyx. There

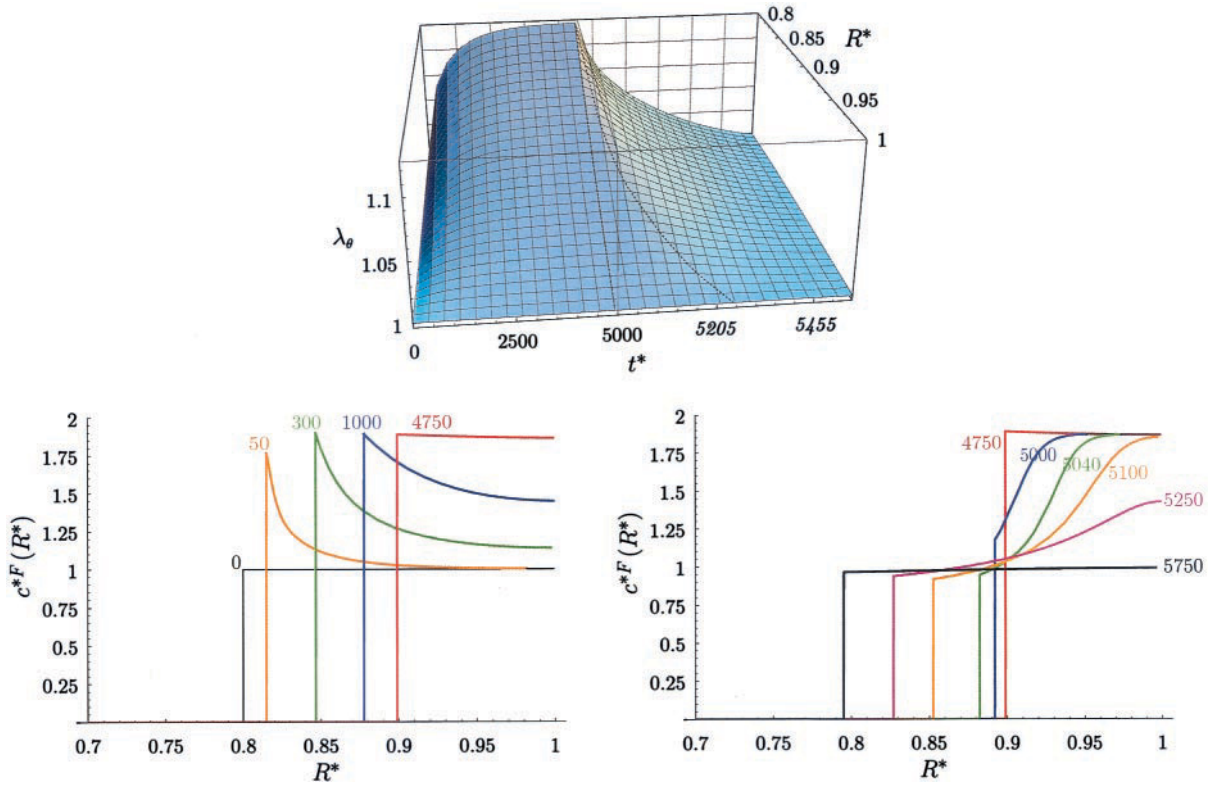

FIGURE 3 Three-dimensional plot (*top*) of the displacement field over space and time for the same parameter values as in Fig. 2 except that $M = 8$. Note that the time scale changes at $t = 5{,}000$, from 500 units per minor axis division to 41 units per division, and this is demarcated by the straight dashed line. Thus compression takes about ten times longer than recovery for this value of M. The dashed curve corresponds to the location of a front where there is a sharp change in the slope of λ_θ. Instantaneous glycocalyx concentration distributions for different times (as indicated beside each curve) during compression (*bottom left*) and recovery (*bottom right*). The concentration front propagating through the glycocalyx during recovery of the matrix is evident in these distributions. Units of time are as in Fig. 2.

are two distinct regimes for the response of the glycocalyx, when $\xi_0^2 \ll \mathcal{F}$ and when $\xi_0^2 \gg \mathcal{F}$, which is evident from both Fig. 4 and Eq. 71. When $\xi_0^2 \ll \mathcal{F}$, the recovery time is essentially independent of ξ_0. In this regime the gradient in the chemical potential is the dominant restoring force. In contrast, when $\xi_0^2 \gg \mathcal{F}$, the recovery time is independent of $\mathcal{F}$, and all the curves of Fig. 4 asymptote to the same function, which rolls off in proportion to ξ_0^{-2}. This is borne

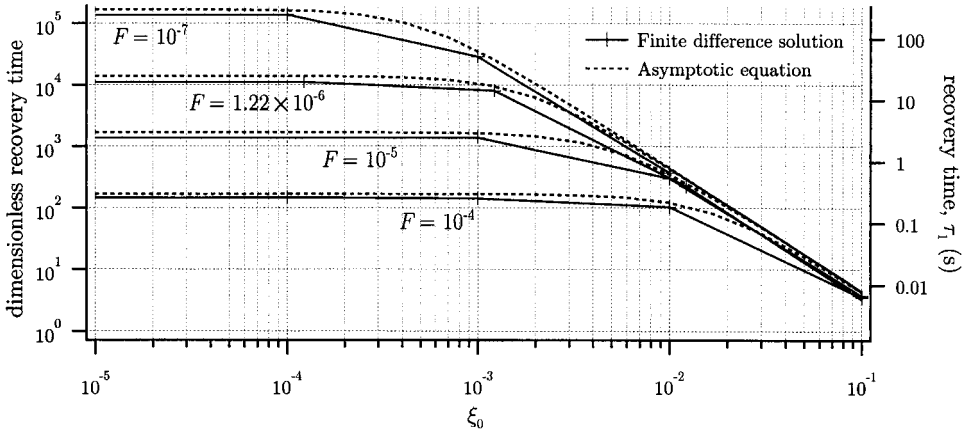

FIGURE 4 The 90% recovery time of the glycocalyx as a function of ξ_0 for different values of $\mathcal{F}$. In all cases $M = 0$, $\alpha_0 = 0.8$, and the maximum applied stress for the numerical results was $\sigma_{ext} = 1$. The form of the asymptotic equation (Eq. 71) agrees very well with the numerical results, and overestimates the recovery time by only ~15%. The dimensional axis on the right of the plot assumes $k_0 = 10^{-11}$ cm^4(dyn-s)$^{-1}$, $c_0^+ = 0.14$ M, and $R_0 = 2.5$ μm.

out in Eq. 71 as well. In this regime, the gradient in the electrostatic potential is the dominant restoring force that drives the recovery. This is important, because it means that only $\mathcal{F}$ or ξ_0 will determine the recovery time, but not both, unless, by chance, it happens that $\xi_0^2 \approx \mathcal{F}$.

Dependence on *M*

The parameter M, associated with the nonlinear strain-dependent permeability, can be investigated only by means of the finite difference solution, because the linearized analysis necessarily ignored it. Figures 2 and 3 show the compression and recovery of the layer for $M = 0$ and $M = 8$, respectively. Because the concentration at the interface where the stress is applied is larger than elsewhere, for the nonlinear case of a strain-dependent permeability given by Eq. B1, where $M > 0$, the permeability achieves a local minimum at the interface. This limits the flux of water into the layer and therefore the rate at which the layer can recover into plasma. Comparing Figs. 2 and 3, we see that when $M = 8$, the compression of the glycocalyx occurs much more slowly for a given applied stress then when $M = 0$. The fact that leukocytes are seen to crush the glycocalyx in capillaries of mammalian skeletal muscle (Vink et al., 1999) would suggest an upper bound on the range of M to include only those values that allow for compression of the matrix over a time interval that is consistent with the time required for a leukocyte to pass. However, in the presence of axial flow that arises through the glycocalyx in a real capillary, deformations imparted to the layer by passing leukocytes would result in axial gradients in the matrix-deformation and permeability fields near the interface that would allow a diversion of the radial flow into the axial direction. Thus, bounds on M cannot be determined from the present analysis. However, the value of M is not expected to exceed values typical of articular cartilage (Lai and Mow, 1980).

Although the compression time is strongly dependent upon the value of M, it is fortunate that the recovery time is relatively insensitive to M. This can be explained by considering the instantaneous glycocalyx concentration distributions that develop during recovery when $M > 0$. Most notable is the front that forms (around $R = 0.9$ in the right panel of Fig. 3) and propagates toward the endothelium as the layer recovers. As this front travels toward the capillary wall, it leaves in its wake a region of relatively low concentration (and correspondingly high permeability) that encounters little drag as it expands into the lumen. For the constant permeability case, when $M = 0$, no front arises. For the larger values of M considered, the front develops at the interface between the glycocalyx and the plasma in the lumen just as the recovery stage begins. The front, which propagates toward the endothelium, and the interface, which travels away from the endothelium, diverge at nearly equal speeds that decrease as time progresses. Thus, the interface is nearly unaffected by the front, and the recovery times associated with cases of strain-dependent permeability and constant permeability are not significantly different. Furthermore, in the presence of axial flow through the glycocalyx of a real capillary, such a front is unlikely because leukocyte-induced axial gradients in the matrix-deformation and permeability fields of the layer would likely relieve, to a large extent, the compression front seen in Fig. 3.

Dependence on α_0

Over the values of α_0 considered, finite difference solutions of Eq. 55 revealed a nearly quadratic dependence of the glycocalyx recovery time on the dimensionless layer thickness, $1 - \alpha_0$ (results not shown). One can see that this result is consistent with the linearized analysis by noting that Eq. 71 is approximately quadratic in $1 - \alpha_0$ for $\alpha_0 \approx 1$.

Comparison between results of finite difference and asymptotic solutions

It is evident from Fig. 4 that recovery times predicted by the finite difference solution to the nonlinear PDE are in good agreement with the result of the linearized analysis for τ_1 given by Eq. 71, at least in terms of the dependence of the recovery time on the parameters ξ_0 and $\mathcal{F}$. The systematic 15% difference between the numerical and asymptotic values can be explained, in part, by the slight ambiguity in the interpretation of numerical results as to precisely where the loading ends and the recovery begins because unloading was simulated by a rapid but smoothly changing function (see Fig. 1) rather than a discontinuous step. In addition, nonlinearities in the PDE that were neglected in the linearized analysis and higher order terms ignored in the asymptotic solution are likely to account for some of the difference as well.

Hysteresis

Figure 5 shows the strain at the luminal interface as a function of applied stress for different loads and loading rates. For the static stress–strain curves, associated with an infinitely long loading rate, loading and unloading follow the same curve. Under dynamic loading, hysteresis is seen in the loading cycle, where the area enclosed by the stress–strain curve is associated with the rate at which energy is dissipated by compressing the glycocalyx. This should roughly correspond to the excess power per unit length of capillary required to force a leukocyte through a glycocalyx-lined rather than smooth-walled capillary of a given diameter. Because axial flow through the capillary is likely to attenuate the hysteresis shown here, we expect that the magnitude of the area enclosed by a given stress–strain curve represents an upper bound on the excess power re-

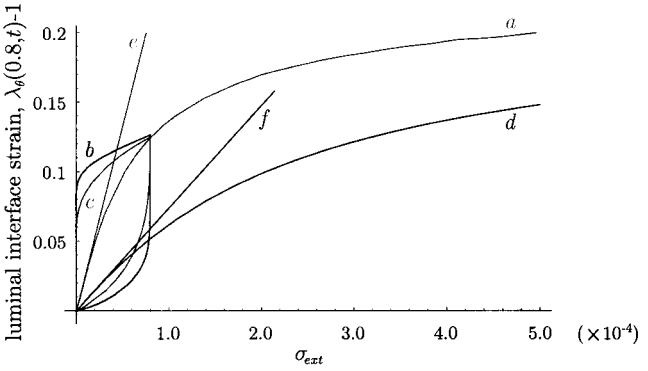

FIGURE 5 The stress–strain curves. Curve *a* is the static stress–strain relation for $\mathcal{F} = 10^{-7}$, $\xi_0 = 0.01$, $M = 0$, and $\alpha_0 = 0.8$. Curves *b* and *c* are hysteresis loops arising from dynamic compression of the layer for the same parameters as in curve *a* with $\tau_{load} = 300$ for curve *b* and 1000 for curve *c*. Both loops are traversed counterclockwise in time. After dynamic compression, both simulations were allowed to relax before beginning the recovery phases, and thus the cusps of both loops lie on the static stress–strain curve. Curve *d* is the static stress–strain curve for $\xi_0 = 0.02$ with all other parameters the same. Straight lines, *e* and *f*, beginning at the origin correspond to the stress–strain relationship predicted by Eq. 70 of the linearized theory. These are seen to be in good agreement with the static stress–strain curves of the nonlinear theory in the limit of small strains. The static stress–strain curves, *a* and *d*, asymptote to 0.25, which corresponds to the limiting value of the luminal interface strain as the glycocalyx approaches zero thickness for $\alpha_0 = 0.8$. The model, however, applies only to finite deformations of the layer for which the solid volume fraction remains small compared with unity. It is noteworthy that curves *a* and *d* would nearly coincide over the entire range of deformations shown if, in both cases, σ_{ext} were scaled by the factor $(2\mathcal{F} + 3/4\xi_0^2)^{-1}$. This self-similarity, which is consistent with Eq. 70 of the linearized theory, is therefore seen to extend to large deformations of the layer. The stresses shown are in units of $k_B T c_0^+$ ($= 3.5 \times 10^6$ dyn/cm^2 for $c_0^+ = 0.14$ M).

quired to overcome the glycocalyx under those loading conditions. This excess power, however, is dependent upon loading rate and therefore leukocyte velocity through the capillary. For low loading rates, the stress–strain curve nearly traces over itself and encloses a small area. Low loading rates, therefore, require little net work over one loading cycle and result in little dissipative energy loss. As the loading rate increases, the area enclosed for a given maximum load is also seen to increase, which reflects the increase in power required to compress the glycocalyx.

DISCUSSION

The close agreement in the predicted recovery times between the finite difference solution and the asymptotic solution given by Eq. 71 lends strong support to the accuracy of both in approximating the solution to the nonlinear diffusion equation given by Eq. 55. Despite the convenience of the asymptotic solution, and the insights we gain from it, at the present time, details of the strain field under finite deformations of the layer can nevertheless be inferred only from the solution of the nonlinear PDE.

It is clear from Eq. 71 and Fig. 4 that, if $\xi_0^2 \gg \mathcal{F}$, then the electrostatic potential, $(n/z^+)\mu^{*+} \sim nO(\xi_0) \sim O(\xi_0^2/\mathcal{F})$, dominates over the chemical potential, $\mu^{*s} \sim O(1)$. If this hypothesis is borne out experimentally, then the glycocalyx fixed-charge density, and not the concentration of the glycocalyx, is the fundamental determinant of the restoring-force capability of the layer.

Parameter estimates based on available experimental data

It is a fortuitous result that the glycocalyx recovery time is relatively insensitive to the precise value of the parameter *M*. However, it varies in inverse proportion to the permeability, k_0. Therefore, experimental measurements of the recovery time of the glycocalyx in the wake of a passing leukocyte can be used to estimate k_0 if the magnitude of the restoring force of the layer, which is dependent upon $\mathcal{F}$ and ξ_0, were known. Alternatively, if the permeability were known, the linearized analysis presented above provides a way of estimating the the parameters $\mathcal{F}$ and ξ_0. Using the estimate of k_0 made by Feng and Weinbaum (2000), and the recovery time of the glycocalyx reported by Vink et al. (1999), the applied stress at the luminal interface can be inferred from the ratio of $\tau_1/\gamma(\alpha_0)$ given by Eq. 72. Because the linearized theory is reasonable for luminal interface strains up to ~0.05, which corresponds to a fractional decrease in glycocalyx thickness of 20% for $\alpha_0 = 0.8$ (see Fig. 5), we take $\gamma(\alpha_0) = 0.05$. Therefore, $\tau_1/\gamma(\alpha_0) = 20$ s for a recovery time $\tau_1 \sim 1$ s (Vink et al., 1999). If we assume $k_0 = 10^{-11}$ cm^4(dyn-s)$^{-1}$ (Feng and Weinbaum, 2000), then, for a 5-μm-diameter capillary with a 0.5-μm-thick glycocalyx, $\alpha_0 = 0.8$, and we find from Eq. 72 that $\sigma_{ext} \approx 50$ dyn/cm^2. This result is consistent with the estimate made by Secomb et al. (2001) that values of σ_{ext} greater than 20 but less than 200 dyn/cm^2 were required to deform the glycocalyx. Using $\sigma_{ext} = 50$ dyn/cm^2 and $\gamma(\alpha_0) = 0.05$ in Eq. 70, or, alternatively, using $k_0 = 10^{-11}$ cm^4(dyn-s)$^{-1}$ and $\tau_1 = 1$ s in Eq. 71, we see that $\xi_0 \approx 0.009$ as we let $\mathcal{F} \to 0$. This is illustrated in Fig. 4 where, for $\xi_0^2 \gg \mathcal{F}$, a dimensional recovery time of 1 s corresponds to $\xi_0 \approx 0.009$. In any case, for this value of k_0, we also see from Fig. 4 an upper bound on $\mathcal{F}$ of $\sim 3 \times 10^{-5}$. For normal saline, which has nearly the same ionic strength as whole blood, we take $z^+ = 1$ and $c_0^+ = 0.14$ M and estimate the glycocalyx fixed-charge density in vivo as $nc_0^F = z^+ c_0^+ \xi_0 \approx 1$ mEq/l. In other words, we estimate that there exists approximately one fixed charge on the glycocalyx for every 100 ions in blood.

We caution, however, that this estimate for ξ_0 is strongly dependent upon the value of k_0 and should, perhaps, be regarded as merely one parameter set that is consistent with all of the existing data on the glycocalyx. Fortunately, the mechano-electrochemical model presented here and the electrochemical model of Stace and Damiano (2001) pro-

vide the inspiration for a number of experiments that would likely provide more definitive estimates of the parameters ξ_0, $\mathcal{F}$, and k_0. Several of these experiments are described below.

Experimental implications of the model

Recall that, even in equilibrium, Eq. 53 predicts the existence of a small voltage differential, ΔV, due to the glycocalyx, from the center of the capillary lumen to the endothelial cell wall. The magnitude of ΔV depends on such factors as the state of deformation of the matrix, the glycocalyx fixed-charge density, and the ionic strength of the plasma. If, on the basis of the preliminary data of Vink et al. (1999), we assume a glycocalyx fixed-charge density of $\sim$1 mEq/1, then, in the equilibrium configuration, ΔV is predicted to be on the order of 0.1 mV in normal saline. From Eq. 53, we see that, for $\xi_0 \ll 1$, ΔV varies approximately linearly with $\xi_0/(\lambda_r\lambda_\theta)$, and thus a 50% compressive strain would result in an approximately two-fold increase in ΔV. Although the presence of such an electric field suggests a method for directly probing the electromechanical properties of the layer, the practical limitations of directly measuring variations in voltage differentials in a 500-nm-thick layer hydrated in normal saline are prohibitive at the present time. The possibility of inducing changes in the equilibrium dimension of the layer or modulating the glycocalyx recovery time by the application of a radially symmetric electric field is also impractical in a 5-μm-diameter capillary.

However, our analysis reveals that the magnitude of $\partial V/\partial R$, and hence the glycocalyx restoring force, can be attenuated by increasing (or amplified by decreasing) the concentration of mobile cations in the plasma. By differentiating Eq. 53, we see that, for $\xi_0 \ll 1$,

$$\frac{\partial V^*}{\partial R^*} \sim -\frac{\xi_0}{2Q}\frac{\partial}{\partial R^*}\left(\frac{f(R^*)}{\lambda_r\lambda_\theta}\right) + O(\xi_0^3/Q). \qquad (75)$$

Thus, if $\mathcal{F} \ll \xi_0^2$, a two-fold increase (decrease) in the ionic strength of the plasma (i.e., in the value of $1/\xi_0$) should result approximately in a two-fold decrease (increase) in the magnitude of the glycocalyx restoring force. Under isoosmolar conditions, such variations in the ionic strength of the plasma would have no effect on the glycocalyx equilibrium dimension or on the permeability of the glycocalyx to water, and, therefore, if $\mathcal{F} \ll \xi_0^2$, a two-fold increase (decrease) in the ionic strength of the plasma should result approximately in a two-fold increase (decrease) in the recovery time of the layer after compression by a passing leukocyte. If, in contrast, $\mathcal{F} \gg \xi_0^2$, Eq. 71 predicts that such changes in the ionic strength in the plasma would have almost no effect on either the glycocalyx restoring force or recovery time. In addition to testing the theory on qualitative grounds, such experiments provide a means of estimating ξ_0 and the permeability, k_0, if they are combined with independent experiments aimed at obtaining an isolated estimate of ξ_0, such as those described by Stace and Damiano (2001).

Axial flow

In the present analysis, we have neglected the effect of flow within the vessel; instead, the glycocalyx matrix passes through a quiescent fluid during compression and recovery. In terms of the results presented here, the presence of a prevailing axial flow will have the most significant bearing on rapid transient compression of the matrix as described earlier. This can be explained by considering a two-dimensional axisymmetric flow for which the fluid-velocity vector is given by $\mathbf{v}^w = v_r^w\hat{\mathbf{e}}_r + v_z^w\hat{\mathbf{e}}_z$. Because the Reynolds number is extremely low in capillaries, the radial and axial fluid-velocity components are coupled only through the continuity equation and indirectly through the pressure. In two-dimensional axisymmetric flow, v_r^w does not vanish identically but must satisfy the continuity equation given by

$$\frac{1}{r}\frac{\partial}{\partial r}(rv_r^w) = -\frac{\partial v_z^w}{\partial z}. \qquad (76)$$

From this, it is evident that, where axial gradients in v_z^w are large, radial gradients in v_r^w are likewise large; such a situation arises near the glycocalyx interface during rapid radial compression of the layer by a passing leukocyte. However, in the wake of a passing leukocyte, these gradients become small compared with radial gradients in v_z^w and a lubrication approximation becomes reasonable. As such, during recovery of the matrix after compression, v_r^w and v_z^w are only weakly coupled and the prevailing axial fluid flow and axial matrix deformations can be effectively superimposed on the radial deformations predicted here. Thus the present analysis has practical application to the problem with axial flow insofar as the recovery time and static strain are concerned. The problem of an axisymmetric two-dimensional flow through the glycocalyx is the subject of future investigations.

APPENDIX A: AXISYMMETRIC ONE-DIMENSIONAL EQUATIONS

Eulerian formulation

In the absence of axial deformations and axial flow, the axisymmetric displacement and velocity fields of the solid constituent reduce to $\mathbf{u}^s = u_r^s(r, t)\hat{\mathbf{e}}_r$ and $\mathbf{v}^s = v_r^s(r, t)\hat{\mathbf{e}}_r$, respectively, and the velocity of the water constituent becomes, $\mathbf{v}^w = v_r^w(r, t)\hat{\mathbf{e}}_r$. The variables (r, θ, z) are the cylindrical Eulerian (spatial) coordinates of a point in the field.

From Eq. 10, the one-dimensional axisymmetric form of the continuity equation can be integrated to provide

$$v_r^w = \frac{f(t)}{r} \equiv 0, \qquad (A1)$$

where we have required that the function of integration, $f(t)$, vanish so that v_r^w remain bounded as $r \to 0$, which is also consistent with the requirement

that $v_r^w(r = R_0, t)$ vanish to meet the boundary condition at the endothelial cell wall corresponding to the surface $r = R_0$. Thus, for purely radial deformations in the axisymmetric case, $\mathbf{v}^w = \mathbf{0}$ and the momentum equations become

$$\frac{v_r^s}{k} = \frac{\partial \sigma_{rr}^E}{\partial r} + \frac{\sigma_{rr}^E - \sigma_{\theta\theta}^E}{r} - k_B T \frac{\partial c^F}{\partial r} - nqc^F E_r \quad a(t) \le r \le R_0 \tag{A2}$$

and

$$\begin{aligned}\frac{v_r^s}{k} &= \frac{\partial p}{\partial r} - k_B T \left(\frac{\partial c^+}{\partial r} + \frac{\partial c^-}{\partial r} + \frac{\partial c^F}{\partial r} \right) \\ &\quad - f_d^+ J_r^+ - f_d^- J_r^- \quad 0 \le r \le R_0 \\ &= \frac{\partial p}{\partial r} - k_B T \frac{\partial c^F}{\partial r} - q(\delta + nc^F) E_r \quad 0 \le r \le R_0, \end{aligned} \tag{A3}$$

where

$$J_r^{\pm} = -D^{\pm} \left(\frac{\partial c^{\pm}}{\partial r} - \frac{z^{\pm} q c^{\pm}}{k_B T} E_r \right) \quad 0 \le r \le R_0. \tag{A4}$$

In Eq. A2, $a(t) = a_0 + u_r(r = a_0, t)$ is the instantaneous radial-coordinate location of the interface between the glycocalyx and the plasma in the lumen, where $a_0 = a(t_0)$ is the value of a in the equilibrium configuration. Throughout the vessel, the mass conservation equations governing the mobile ions are given by

$$\frac{1}{D^{\pm}} \frac{Dc^{\pm}}{Dt} = \frac{1}{r} \frac{\partial}{\partial r} (r J_r^{\pm}) \quad 0 \le r \le R_0. \tag{A5}$$

In axisymmetric form, for a purely radially directed electric field, Gauss's law given by Eq. 13 is integrable. Using the global charge neutrality condition, $E_r(R_0, t) = 0$, the nonvanishing component of the electric field may be written as

$$E_r(r, t) = \frac{1}{r} \int_0^r \frac{q\delta(\sigma, t)}{\epsilon} \sigma \, d\sigma = -\frac{1}{r} \int_r^{R_0} \frac{q\delta(\sigma, t)}{\epsilon} \sigma \, d\sigma, \tag{A6}$$

where $\delta(r, t) = z^+ c^+(r, t) + z^- c^-(r, t) - nc^F(r, t)$.

Lagrangian formulation

We seek to transform Eq. A2, which is expressed in spatial coordinates, into its representation in reference coordinates. The purely radial axisymmetric deformations considered here represent a principal state of strain in which material points are displaced only along radial coordinate lines. Under this loading configuration, the cylindrical Lagrangian (reference) coordinates (R, Θ, Z) are related to the Eulerian (spatial) coordinates (r, θ, z) according to

$$r(R, t) = R + U_R(R, t) \quad \theta = \Theta \quad z = Z. \tag{A7}$$

The transformation given above leads to a diagonal deformation gradient tensor, $\mathbf{F} = \partial \mathbf{x}/\partial \mathbf{X}$. Thus, the principal stretch ratios, λ_r, λ_θ, and λ_z, corresponding to the eigenvalues of the left Cauchy–Green deformation tensor, $\mathbf{B} = \mathbf{F}(\mathbf{F})^T$, are given by

$$\lambda_r(R, t) = \frac{\partial r}{\partial R} = 1 + \frac{\partial U_R}{\partial R}$$

$$\lambda_\theta(R, t) = \frac{r}{R} = 1 + \frac{U_R}{R} \quad \lambda_z = 1. \tag{A8}$$

Writing Eq. A2 in reference coordinates and applying the chain rule, we obtain the nonlinear momentum equation given by

$$\frac{1}{k} \frac{\partial U_R}{\partial t} = \frac{1}{\lambda_r} \frac{\partial \sigma_{rr}^E}{\partial R} + \frac{\sigma_{rr}^E - \sigma_{\theta\theta}^E}{R\lambda_\theta} - k_B T \frac{1}{\lambda_r} \frac{\partial c^F}{\partial R} - nqc^F E_r \quad a_0 \le R \le R_0 \tag{A9}$$

and the conservation of mass for the ions given by

$$\frac{\lambda_r \lambda_\theta}{D^{\pm}} \frac{\partial c^{\pm}}{\partial t} = \frac{1}{R} \frac{\partial}{\partial R} \left(\frac{\lambda_\theta}{\lambda_r} R \frac{\partial c^{\pm}}{\partial R} - \frac{z^{\pm} q}{k_B T} R \lambda_\theta c^{\pm} E_r \right) \quad 0 \le R \le R_0. \tag{A10}$$

In material coordinates, the flux of ions is given by

$$J_r^{\pm}(R, t) = -D^{\pm} \left(\frac{1}{\lambda_r} \frac{\partial c^{\pm}}{\partial R} - \frac{z^{\pm} q}{k_B T} c^{\pm} E_r \right) \quad 0 \le R \le R_0, \tag{A11}$$

where

$$E_r(R, t) = -\frac{q}{\epsilon} \frac{1}{R\lambda_\theta} \int_R^{R_0} \delta(\tilde{R}, t) \lambda_r \lambda_\theta \tilde{R} \, d\tilde{R} \tag{A12}$$

and

$$\delta(R, t) = z^+ c^+(R, t) + z^- c^-(R, t) + z^F c^F(R, t). \tag{A13}$$

In terms of the principal stretch ratios, the Jacobian of the deformation gradient tensor, $\mathbf{F}$, is simply $\mathbf{J} = \det \mathbf{F} = \lambda_r \lambda_\theta \lambda_z$. Thus, by the conservation of mass for the solid constituent given by Eq. 11, the glycocalyx concentration is kinematically related to the principal stretch ratios according to

$$c^{*F} = \frac{c^F(R, t)}{c_0^F} = \frac{f(R)}{\lambda_r \lambda_\theta}. \tag{A14}$$

We define $c^F(R, t_0) = c_0^F f(R)$ where c_0^F denotes the maximum glycocalyx concentration in the reference configuration, and $f(R)$ is the normalized shape of the concentration distribution of the glycocalyx in the reference configuration, such that $0 \le f(R) \le 1$. From Eq. A8, we can invoke the kinematic relationships

$$\frac{\partial U_R}{\partial t} = \frac{\partial (R\lambda_\theta)}{\partial t} \quad \text{and} \quad \lambda_r = \frac{\partial (R\lambda_\theta)}{\partial R}, \tag{A15}$$

and express the momentum equation in terms of λ_θ rather than U_R. This results in the nonlinear diffusion equation given by

$$\frac{\lambda_r}{k}\frac{\partial(R\lambda_\theta)}{\partial t} = \frac{\partial \sigma_{rr}^E}{\partial R} + \frac{\lambda_r}{\lambda_\theta}\frac{\sigma_{rr}^E - \sigma_{\theta\theta}^E}{R} - k_B T c_0^F \frac{\partial}{\partial R}\left(\frac{f(R)}{\lambda_r\lambda_\theta}\right) + \frac{nq^2 c_0^F}{\epsilon}\frac{f(R)}{R\lambda_\theta^2}\int_R^{R_0} \delta(\tilde{R}, t)\lambda_r\lambda_\theta \tilde{R}\, d\tilde{R}$$

$$a_0 \le R \le R_0, \quad \text{(A16)}$$

where δ is given by Eq. A13.

APPENDIX B: STRAIN-DEPENDENT CONSTITUTIVE RELATIONS FOR THE SOLID MATRIX

Strain-dependent permeability of the glycocalyx

In the case of finite deformations of the glycocalyx, we assume that the permeability, k, decreases exponentially with compression, and that the argument of the exponential is proportional to the fractional change in volume of the mixture. However, because of the nonlinear kinematics associated with finite deformations of the matrix, the fractional change in volume is, itself, a nonlinear function of the deformation and is related to $I_3 = \lambda_r^2\lambda_\theta^2\lambda_z^2$, where I_3 is the third principal invariant of the left Cauchy–Green deformation tensor, **B**. For the deformations considered here, we invoke the two-parameter constitutive relationship for $k = k(\lambda_r, \lambda_\theta)$ proposed by Lai and Mow (1980) given by

$$k = k_0 e^{M(\lambda_r\lambda_\theta - 1)}, \quad \text{(B1)}$$

where k_0 is the undeformed glycocalyx permeability defined before and M characterizes the sensitivity of the permeability to the local strain field.

The strain energy function for the glycocalyx matrix

Although the fluid constituent is modeled as intrinsically incompressible, the mixture as a whole, with boundaries corresponding to the deformed configuration of the solid matrix, is highly compressible. Approximating the glycocalyx matrix as an isotropic, compressible, hyperelastic material, the strain energy function $W = W(\lambda_r, \lambda_\theta, \lambda_z)$. Although empirical determination of the precise dependence of W on the principal stretch ratios is impractical, we can place restrictions on it that are consistent with the assumptions we have made about the layer. In particular, because we have assumed that the glycocalyx matrix can support only tension and not compression, we require that the radial stress, σ_{rr}, decrease with decreasing λ_r and that the hoop stress, $\sigma_{\theta\theta}$, increase with increasing λ_θ. Furthermore, we assume that an isotropic state of tensile prestress exists in the reference configuration (when $\lambda_r = \lambda_\theta = 1$) such that $\sigma_{rr}(R, t_0) = \sigma_{\theta\theta}(R, t_0)$. These restrictions cannot be met if W were to depend only upon I_3, the third principal invariant of the left Cauchy–Green deformation tensor, **B**. However, strain energy functions that depend only upon the first, I_1, or second, I_2, principal invariants are admissible. The form of the strain energy function and stress components for this deformation are similar but more complicated if we assume I_2 dependence. Therefore, to avoid contrived specificity, we assume the simplest possible form for which $W = W(I_1)$ only. For the purely radial deformations considered here, $\lambda_z = 1$ and $I_1 = \lambda_r^2 + \lambda_\theta^2 + 1$. In this case, the stress response for an isotropic, compressible, hyperelastic material that satisfies the principle of material frame indifference is given by

$$\boldsymbol{\sigma}^E = \frac{1}{\lambda_r\lambda_\theta}\left(\frac{1}{\lambda_r}\frac{\partial W}{\partial \lambda_r} + \frac{1}{\lambda_\theta}\frac{\partial W}{\partial \lambda_\theta}\right)\mathbf{B}, \quad \text{(B2)}$$

where **B** is diagonal for this principal state of strain with elements λ_r^2, λ_θ^2, and 1. The corresponding radial and circumferential components of stress are then given by

$$\sigma_{rr}^E(R, t) = \frac{\lambda_r}{\lambda_\theta}\left(\frac{1}{\lambda_r}\frac{\partial W}{\partial \lambda_r} + \frac{1}{\lambda_\theta}\frac{\partial W}{\partial \lambda_\theta}\right)$$

and

$$\sigma_{\theta\theta}^E(R, t) = \frac{\lambda_\theta}{\lambda_r}\left(\frac{1}{\lambda_r}\frac{\partial W}{\partial \lambda_r} + \frac{1}{\lambda_\theta}\frac{\partial W}{\partial \lambda_\theta}\right). \quad \text{(B3)}$$

The simplest constitutive relationship that meets the restrictions stated above and satisfies Eq. B3 has the strain energy function and stress response given by

$$W(\lambda_r, \lambda_\theta) = \tfrac{1}{4}T_0(R)(\lambda_r^2 + \lambda_\theta^2 + 1),$$

$$\sigma_{rr}^E = T_0(R)\frac{\lambda_r}{\lambda_\theta}, \quad \text{and} \quad \sigma_{\theta\theta}^E = T_0(R)\frac{\lambda_\theta}{\lambda_r}, \quad \text{(B4)}$$

where $T_0(R)$ is the tensile prestress that balances the electrochemical forces in the equilibrium configuration. Lacking specific data about glycocalyx constitutive behavior, a more complicated model cannot be justified at the present time. It should be noted, however, that, insofar as the recovery time and recovery dynamics of the layer are concerned, Eq. B4 is sufficiently nonlinear to render the mechanical stresses negligibly small for all but the very smallest deformations. A constitutive relationship that is more strongly nonlinear than Eq. B4 would yield substantially equivalent results. Therefore, knowledge of the precise form of the strain energy function is not necessary, as long as the mechanical terms only become important very near equilibrium. This criterion is indeed met by the proposed strain energy function given by Eq. B4.

APPENDIX C: BOUNDARY CONDITIONS

The axisymmetric assumption requires that all gradients, including the concentration gradients of mobile ions and the electric field (i.e., the voltage gradient), vanish along the centerline of the capillary at $r = 0$. We further assume global charge neutrality, such that $E_r(r = R_0, t) = 0$, and zero flux of cations and anions across the endothelial cell membrane at $r = R_0$, such that $J_r^{\pm}(r = R_0, t) = 0$. Substituting these two boundary conditions at $r = R_0$ into the expression for $J_r^{\pm}$ given by Eq. A4, we obtain

$$\left.\frac{\partial c^{\pm}}{\partial r}\right|_{r=R_0} = 0. \quad \text{(C1)}$$

In addition, the velocity field associated with the water constituent and the displacement field associated with the solid constituent are taken to vanish at $r = R_0$, such that $v_r^w(r = R_0, t) = 0$ and $u_r^s(r = R_0, t) = 0$.

The boundary condition at the interface between the glycocalyx and the plasma in the lumen requires special consideration of the conservation equations integrated over a surface of material discontinuity. We denote $\Gamma(t)$ as this interfacial cylindrical surface, defined by $r = a(t)$, and refer to the jump discontinuity in a quantity $\phi(r, t)$ across $\Gamma(t)$ as $[\![\phi]\!] \equiv \phi(a^+(t)) - \phi(a^-(t))$. To simulate the effect of an externally applied, time-varying

stress–traction imposed by a passing cell, we generalize the momentum equation for the solid constituent by adding to the right-hand side of Eq. A2, a stress–traction vector, $\mathbf{t}_{\text{ext}} = t_{\text{ext}}(t)\delta(r - a(t))\hat{\mathbf{e}}_r$, which acts uniformly over $\Gamma(t)$. The function $t_{\text{ext}}(t)$ can be regarded as the radial normal component of the stress–traction exerted by a passing cell. Because only radial deformations are considered in this analysis, the shear component will be neglected. We arrive at the boundary condition at $r = a(t)$ by integrating Eqs. A2–A4 over the interval $a(t) - \varepsilon \le r \le a(t) + \varepsilon$, which contains $\Gamma(t)$, and then passing to the limit as $\varepsilon \to 0$. Noting that the radial velocity component, v_r^s, of the solid constituent is bounded and continuous across $\Gamma(t)$, and that the stress components, σ_{rr}^E and $\sigma_{\theta\theta}^E$, contain only a bounded step discontinuity across $\Gamma(t)$, the integrals of these terms across $\Gamma(t)$ vanish as $\varepsilon \to 0$, and we are left with

$$t_{\text{ext}}(t) = [\![-\sigma_{rr}^E + k_B T c^F]\!] + \int_{a^-(t)}^{a^+(t)} nqc^F(r, t)E_r(r, t)\, dr, \tag{C2}$$

$$[\![p]\!] = [\![k_B T c^F]\!] + \int_{a^-(t)}^{a^+(t)} q(\delta(r, t) + nc^F(r, t))E_r(r, t)\, dr, \tag{C3}$$

and

$$[\![f_d^{\pm} J_r^{\pm}]\!] = [\![-k_B T c^{\pm}]\!] + \int_{a^-(t)}^{a^+(t)} z^{\pm} qc^{\pm}(r, t)E_r(r, t)\, dr. \tag{C4}$$

APPENDIX D: LINEARIZED ANALYSIS FOR SMALL STRAINS

The linearized equation is given by Eq. 69. To obtain a solution for the recovery time of the layer in the absence of an externally applied stress (corresponding to the recovery of the glycocalyx into cell-free plasma), we invoke the boundary condition given by Eq. 67 and take $t_{\text{ext}} = 0$. To derive a result for the steady-state strain, in contrast, we will retain t_{ext} but set the time derivative in Eq. 69 to zero. Throughout this section, dimensionless variables will be used, however the asterisk will be omitted for brevity.

Assuming $f(R) = 1$ on $\alpha_0 < R \le 1$, and recalling that both λ_r and λ_θ are positive, in the small-strain limit, the power series expansion of Eq. 67, in terms of $\Delta\lambda$, is given by

$$\left\{T_0(\alpha_0) - 1 + \frac{1}{\mathcal{F}}(2 - \sqrt{\xi_0^2 + 4})\right\} + \frac{2}{\mathcal{F}}\left(\mathcal{F} + \frac{\xi_0^2}{\sqrt{\xi_0^2 + 4}}\right)\Delta\lambda(\alpha_0, t) + \frac{2\alpha_0}{\mathcal{F}}\left(\mathcal{F} - 1 + \frac{2 + \xi_0^2}{\sqrt{\xi_0^2 + 4}}\right)\frac{\partial(\Delta\lambda)}{\partial R}\bigg|_{R=\alpha_0} + \cdots = -t_{\text{ext}}(t), \tag{D1}$$

where all neglected terms are quadratic or higher order in $\Delta\lambda$ or contain nonlinear products of $\Delta\lambda$ and its derivatives. We see that, according to Eq. 68, the quantity in braces on the left-hand side of Eq. D1 vanishes. Thus, the linearized interfacial boundary condition at $R = \alpha_0$ is homogeneous and may be written as

$$\Delta\lambda(\alpha_0, t) + \beta\frac{\partial(\Delta\lambda)}{\partial R}\bigg|_{R=\alpha_0} = -\frac{t_{\text{ext}}(t)}{\chi}, \tag{D2}$$

where

$$\beta = \alpha_0\left(1 + \frac{2 - \sqrt{\xi_0^2 + 4}}{\xi_0^2 + \mathcal{F}\sqrt{\xi_0^2 + 4}}\right) \approx \alpha_0\left(\frac{1 + 3\xi_0^2/8\mathcal{F}}{1 + \xi_0^2/2\mathcal{F}}\right)$$

and

$$\chi = \frac{2}{\mathcal{F}}\left(\mathcal{F} + \frac{\xi_0^2}{\sqrt{\xi_0^2 + 4}}\right). \tag{D3}$$

Note that the approximate equality given above for β corresponds to the (3,3)-Pade approximant of β. It is clear from this expression for β that $\frac{3}{4} < \beta/\alpha_0 < 1$ for all values of $\xi_0^2/\mathcal{F}$. In terms of $\Delta\lambda$, the boundary condition at $R = 1$, given by Eq. 62, is simply

$$\Delta\lambda(1, t) = 0. \tag{D4}$$

The linearized boundary-value problem defined by Eqs. 69, D2, and D4 can be recognized as a Sturm–Liouville problem with weight function $w(R) = R$.

We seek a multiplicatively separable solution to the linearized PDE of the form $\Delta\lambda(R, t) = \gamma(R)\varphi(t)$ and separate variables in time and space. The separated form of Eq. 69 is

$$\sqrt{\frac{D^+}{D_0^F}}\frac{\dot{\varphi}(t)}{\varphi(t)} = \frac{2}{\mathcal{F}}\left(\mathcal{F} - 1 + \frac{2 + \xi_0^2}{\sqrt{4 + \xi_0^2}}\right) \times \frac{1}{\gamma(R)}\left(\frac{3}{R}\gamma'(R) + \gamma''(R)\right) = -\eta^2, \tag{D5}$$

where dots and primes denote temporal and spatial derivatives, respectively, and the constant η is determined from the boundary conditions. Substituting $\gamma(R)\varphi(t)$ for $\Delta\lambda(R, t)$ in Eqs. D2 and D4, we find that the boundary conditions on γ are

$$\gamma(\alpha_0) + \beta\gamma'(\alpha_0) = -\frac{t_{\text{ext}}(t)}{\chi} \quad \text{and} \quad \gamma(1) = 0. \tag{D6}$$

The spatial ordinary differential equation (ODE), corresponding to the second of Eq. D5, can be written as

$$\gamma'' + \frac{3}{R}\gamma' + \nu^2\gamma = 0, \tag{D7}$$

where we have introduced the new constant

$$\nu^2 \equiv \eta^2\left[\frac{2}{\mathcal{F}}\left(\mathcal{F} - 1 + \frac{2 + \xi_0^2}{\sqrt{4 + \xi_0^2}}\right)\right]^{-1}. \tag{D8}$$

Maximum strain

We are interested here in the steady-state solution to the linearized ODE given by Eq. D7. This is given by the zeroth-order eigenfunction, which is determined from Eq. D7 by setting $\nu = 0$, for then the temporal eigen-

function is $e^{-\nu^2 t} = 1$, so that $\gamma(R) = \Delta\lambda(R, \infty)$ is the total relative strain at R. The solution to Eq. D7 for the case $\nu = 0$ is

$$\gamma(R) = \frac{(1 - R^2)\sigma^*_{\text{ext}}\alpha_0^3}{R^2\chi(2\beta - \alpha_0 + \alpha_0^3)}, \tag{D9}$$

where $\sigma_{\text{ext}} = \max(t_{\text{ext}}(t))$ is the maximum value the applied stress–traction reaches during the load cycle. We are interested in the maximum strain, which occurs at $R = \alpha_0$, so we make this replacement. The resulting expression can be simplified somewhat by recognizing that $\alpha_0 \lesssim 1$, so expanding in the neighborhood of $\alpha_0 = 1$ results in

$$\gamma(\alpha_0) = \frac{(1 - \alpha_0)\sigma_{\text{ext}}}{k_B T c_0^+ (2\mathcal{F} + \frac{3}{4}\xi_0^2)} + O((1 - \alpha_0)^2). \tag{D10}$$

The leading-order term corresponds to the right-hand side of Eq. 70. In deriving this expression, we have also made the replacement $\sqrt{4 + \xi_0^2} \to 2$, because $\xi_0 \ll 1$.

Recovery time

We now turn to the recovery time, which can be determined from the eigenvalue problem given by Eq. D7 when the eigenvalue, ν, is nonzero. Because we are interested in recovery of the layer into cell-free plasma, we set $t_{\text{ext}} = 0$ in the boundary condition given by Eq. D2. In terms of Bessel functions, the solution to Eq. D7 is given by

$$\gamma(R) = a\,\frac{Y_1(\nu R)}{R} + b\,\frac{J_1(\nu R)}{R}, \tag{D11}$$

where a and b are constants and $J_1(x)$ and $Y_1(x)$ are first-order Bessel functions of the first and second kind, respectively. This solution is substituted into the two boundary conditions given by Eq. D6, and, because we require that neither a nor b vanish, we obtain a characteristic equation whose roots are the eigenvalues of the problem. This characteristic equation is found to be

$$Y_1(\nu)(J_1(\alpha_0\nu) - \beta\nu J_2(\alpha_0\nu)) - J_1(\nu)(Y_1(\alpha_0\nu) - \beta\nu Y_2(\alpha_0\nu)) = 0. \tag{D12}$$

The roots of Eq. D12 form a denumerable infinite set, $\{\nu_n\}_{n=1}^{\infty}$, where ν_n are related to the eigenvalues, η_n, of the problem through Eq. D8. These eigenvalues are physically important because they determine the $1/e$ decay times, $(\tau_{e^{-1}})_n = \eta_n^{-2}$, that are each associated with a corresponding spatial eigenfunction, $\gamma_n(R)$. In general, the lowest positive eigenvalue, η_1, is the most physically important because it determines the longest characteristic time of the problem. We note that the lowest eigenvalue is strictly positive, because, if $\eta_0 = 0$ were an eigenvalue, the solution to Eq. D7 would be given by $\gamma_0(R) = a_0 + b_0/R^2$, which can be made to satisfy the boundary conditions given by Eq. D6 if and only if $\beta/\alpha_0 = (1 - \alpha_0^2)/2 < 1/2$; this, however, contradicts the fact that $\beta/\alpha_0 > 3/4$. Therefore, $\eta_0 = 0$ is not an eigenvalue.

The characteristic equation depends transcendentally on ν, so we have no analytic expressions for its roots, however we can obtain a very good estimate of the first positive root of Eq. D12 by expanding it in a Taylor series to $O(\nu^5)$ and finding the first positive root of the truncated series. The characteristic equation is an even function of ν, so the Taylor series has only even powers of ν, and the truncated series is quadratic in ν^2. Even though the first positive root of Eq. D12 is not necessarily small compared with unity, the left-hand side of Eq. D12 is a fairly smooth function of ν up to its first root, so the truncated series does represent a good approximation of Eq. D12 at least as far as the first root. The roots of the truncated series are quite lengthy so we do not include them here. Instead, we refer to them as $\tilde{\nu}_n(\alpha_0, \beta)$, where the tilde is to indicate that these roots correspond to the truncated series and are an approximation to that of the actual roots, ν_n, of Eq. D12. Because $\alpha_0 \lesssim 1$, we expand the root about $\alpha_0 = 1$ and obtain

$$\tilde{\nu}_1(\alpha_0, \beta) = \frac{\sqrt{6 - \sqrt{12}}}{1 - \alpha_0} + \sqrt{\frac{3}{50} + \frac{1}{\sqrt{300}}}\left(\frac{3\beta - 2}{\beta}\right) + O(1 - \alpha_0) \approx \frac{1.592}{1 - \alpha_0} + 0.343\left(\frac{3\beta - 2}{\beta}\right). \tag{D13}$$

We note that the term depending on β in this equation is included for completeness. However, because it is $O(1)$ to highest order in $1 - \alpha_0$, it can be neglected without significant loss in accuracy, which we shall do hereafter. This formula provides a good estimate of the first positive root of Eq. D12, and therefore of the first positive eigenvalue. Recalling the definition of ν^2 given by Eq. D8, we use this result to obtain the following expression for η_1^2 in terms of ξ_0, $\mathcal{F}$, and α_0:

$$\eta_1^2 \approx \frac{2}{\mathcal{F}}\left(\mathcal{F} - 1 + \frac{2 + \xi_0^2}{\sqrt{4 + \xi_0^2}}\right)\frac{6 - \sqrt{12}}{(1 - \alpha_0)^2}. \tag{D14}$$

The time-dependent Fourier coefficient associated with the first nonzero eigenvalue is given by the solution to the time-dependent equation in Eq. D5. To within an arbitrary constant, this is given by

$$\varphi_1(t) = \exp\left(-\sqrt{\frac{D_0^F}{D^+}}\,\eta_1^2 t\right). \tag{D15}$$

The dimensional 90% recovery time, τ_1, associated with the first positive eigenvalue is related to the $1/e$ time by $\tau_1 = \ln(10)(\tau_{e^{-1}})_1$. From the argument of the exponential in Eq. D15, we have

$$\tau_1 = \ln(10)\tau_c\,\frac{\sqrt{D^+/D_0^F}}{\eta_1^2} = \frac{\ln(10)R_0^2}{D_0^F\eta_1^2} = \left(\frac{R_0^2}{k_0 k_B T c_0^+}\right)\frac{\ln(10)}{\mathcal{F}\eta_1^2}. \tag{D16}$$

In keeping with our assumption that $\mathcal{F} \ll 1$ and $\xi_0 \ll 1$, we expand the middle factor of Eq. D14 in both ξ_0 and $\mathcal{F}$ and discard terms that are higher than $O(\xi_0^2)$ and $O(\mathcal{F})$. Substituting the resulting expression for η_1^2 into Eq. D16 gives

$$\tau_1 \approx \left(\frac{R_0^2}{k_0 k_B T c_0^+}\right)\frac{\ln(10)(1 - \alpha_0)^2}{(2\mathcal{F} + \frac{3}{4}\xi_0^2)(6 - \sqrt{12})}. \tag{D17}$$

Partial support for this work was provided by the Whitaker Foundation (Grant RG-98-0524).

REFERENCES

Barry, S. I., K. H. Parker, and G. K. Aldis. 1991. Fluid flow over a thin deformable porous layer. *J. Appl. Math. Phys.* 42:633–648.

Bockris, J. O. M., and A. K. N. Reddy. 1970. Modern Electrochemistry. Vol. 1. Plenum Press, New York.

Bowen, R. M. 1976. Theory of mixtures. *In* Continuum Physics. A. C. Eringen, editor. Academic, New York. 1–127.

Copley, A. L. 1974. Hemorheological aspects of the endothelium-plasma interface. *Microvasc. Res.* 8:192–212.

Damiano, E. R. 1998. The effect of the endothelial-cell glycocalyx on the motion of red cells through capillaries. *Microvasc. Res.* 55:77–91.

Damiano, E. R., B. R. Duling, K. Ley, and T. C. Skalak. 1996. Axisymmetric pressure-driven flow of rigid pellets through a cylindrical tube lined with a deformable porous wall layer. *J. Fluid Mech.* 314:163–189.

Desjardins, C., and B. R. Duling. 1990. Heparinase treatment suggests a role for the endothelial cell glycocalyx in regulation of capillary hematocrit. *Am. J. Physiol. Heart Circ. Physiol.* 264:H909–H916.

Feng, J., and S. Weinbaum. 2000. Lubrication theory in highly compressible porous media: the mechanics of skiing, from red cells to humans. *J. Fluid Mech.* 422:281–317.

Henry, C. B. S., and B. R. Duling. 1999. Permeation of the luminal capillary glycocalyx is determined by hyaluronan. *Am. J. Physiol. Heart Circ. Physiol.* 277:H508–H514.

Henry, C. B. S., and B. R. Duling. 2000. TNF-α increases entry of macromolecules into luminal endothelial cell glycocalyx. *Am. J. Physiol. Heart Circ. Physiol.* 279:H2815–H2823.

Katchalsky, A., and P. F. Curran. 1965. Nonequilibrium Thermodynamics in Biophysics. Harvard University Press, Cambridge, MA.

Klitzman, B., and B. R. Duling. 1979. Microvascular hematocrit and red cell flow in resting and contracted striated muscle. *Am. J. Physiol. Heart Circ. Physiol.* 237:H481–H490.

Krindel, P., and A. Silberberg. 1979. Flow through gel-walled tubes. *J. Coll. Inter. Sci.* 71:39–50.

Lahav, J., N. Eliezer, and A. Silberberg. 1973. Gel-walled cylindrical channels as models for the microcirculation: dynamics of flow. *Biorheology.* 10:595–604.

Lai, W. M., J. S. Hou, and V. C. Mow. 1991. A triphasic theory for the swelling and deformation behaviors of articular cartilage. *J. Biomech. Eng.* 113:245–258.

Lai, W. M., and V. C. Mow. 1980. Drag induced compression of articular cartilage during a permeation experiment. *Biorheology.* 17:111–123.

Mow, V. C., S. C. Kuei, W. M. Lai, and C. G. Armstrong. 1980. Biphasic creep and stress-relaxation of articular cartilage in compression: theory and experiment. *J. Biomech. Eng.* 102:73–84.

Needham, D., and R. M. Hochmuth. 1990. Rapid flow of passive neutrophils into a 4μm pipet and measurement of cytoplasmic viscosity. *J. Biomech. Eng.* 112:269–276.

Özkaya, N. 1986. Viscous flow of particles in tubes: lubrication theory and finite element models. Ph.D. Thesis, Columbia University, New York, NY.

Pries, A. R., T. W. Secomb, T. Gessner, M. B. Sperandio, J. F. Gross, and P. Gaehtgens. 1994. Resistance to blood flow in microvessels in vivo. *Circ. Res.* 75:904–915.

Pries, A. R., T. W. Secomb, H. Jacobs, M. B. Sperandio, K. Osterloh, and P. Gaehtgens. 1997. Microvascular blood flow resistance: role of endothelial surface layer. *Am. J. Physiol. Heart Circ. Physiol.* 273: H2272–H2279.

Robinson, R. A., and R. H. Stokes. 1955. Electrolyte Solutions. Butterworths Scientific Publications, London.

Secomb, T. W. 1995. Mechanics of blood flow in the microcirculation. *In* Biological Fluid Dynamics. C. P. Ellington and T. J. Pedley, editors. Company of Biologists, Cambridge, U.K. 305–321.

Secomb, T. W., and J. F. Gross. 1983. Flow of red blood cells in narrow capillaries: role of membrane tension. *Int. J. Microcirc. Clin. Exp.* 2:229–240.

Secomb, T. W., R. Hsu, and A. R. Pries. 1998. A model for red blood cell motion in glycocalyx-lined capillaries. *Am. J. Physiol. Heart Circ. Physiol.* 274:H1016–H1022.

Secomb, T. W., R. Hsu, and A. R. Pries. 2001. Motion and deformation of red blood cells in a capillary with an endothelial surface layer: effect of flow velocity. *Am. J. Physiol. Heart Circ. Physiol.* 281:H629–H636.

Secomb, T. W., R. Skalak, N. Özkaya, and J. F. Gross. 1986. Flow of axisymmetric red blood cells in narrow capillaries. *J. Fluid Mech.* 163:405–423.

Skalak, R., and N. Özkaya. 1987. Models of erythrocyte and leukocyte flow in capillaries. *In* Physiological Fluid Dynamics II. L. S. Srinath and M. Singh, editors. Tata McGraw-Hill, New Delhi, India. 1–10.

Stace, T. M., and E. R. Damiano. 2001. An electrochemical model of the transport of charged molecules through the capillary glycocalyx. *Biophys. J.* 80:1670–1690.

Tombs, M. P., and A. R. Peacocke. 1974. The Osmotic Pressure of Biological Macromolecules. Clarendon Press, Oxford, U.K.

Truesdell, C., and R. Toupin. 1960. The classical field theories. *In* Handbuch der Physik. S. Flügge, editor. Springer-Verlag, Berlin. 226–793.

Vink, H., and B. R. Duling. 1996. Identification of distinct luminal domains for macromolecules, erythrocytes, and leukocytes within mammalian capillaries. *Circ. Res.* 79:581–589.

Vink, H., and B. R. Duling. 2000. The capillary endothelial surface layer selectively reduces plasma solute distribution volume. *Am. J. Physiol. Heart Circ. Physiol.* 278:H285–H289.

Vink, H., J. A. E. Spaan, and B. R. Duling. 1999. Mechanical properties of the endothelial surface layer. *FASEB J.* 13:A11 (Abstr).

Wang, H., and K. H. Parker. 1995. The effect of deformable porous surface layers on the motion of a sphere in a narrow cylindrical tube. *J. Fluid Mech.* 283:287–305.

Zarda, P. R., S. Chien, and R. Skalak. 1977a. Elastic deformations of red blood cells. *J. Biomech.* 10:211–221.

Zarda, P. R., S. Chien, and R. Skalak. 1977b. Interaction of a viscous incompressible fluid with an elastic body. *In* Computational Methods for Fluid–Solid Interaction Problems. T. Belytschko and T. L. Geers, editors. American Society of Mechanical Engineers, New York. 65–82.